

A 5 Electronic structure of matter: Reduced dimensions

Stefan Blügel

Institut für Festkörperforschung

Forschungszentrum Jülich

Contents

1	Introduction	2
1.1	Electrons in a periodic potential: single electron picture	2
2	Confined Electronic States	3
2.1	Jellium Model	4
2.2	Quantum-Well States	6
3	Electronic Structure of Surfaces	9
3.1	Qualitative Discussion in One Dimension	10
3.2	Description in Three Dimensions	12
3.3	Metallic Surfaces	13
3.4	Semiconductor Surfaces	19
4	Transition Metals in Reduced Dimensions: Magnetism	21
4.1	Role of Coordination Number	23
4.2	Low-Dimensional Magnets	27

1 Introduction

In this lecture we discuss the consequences for the electronic structure of a crystalline solid if one or more dimensions of the system size are reduced, reduced to a level where measurable quantities are modified. This includes the change of the quantization conditions for an electron wave due to the presence of new boundary conditions which alters the eigenvalue spectrum and thus the transport and other properties of the solid. This is well-understood in terms of a single electron picture. With the reduced dimensions, the symmetries of the system are lowered, surfaces and interfaces move into the focus of attention and the appearance of new boundary conditions lead to additional states, called surface states and interface states. Typical for solids at reduced dimensions is also the reduction of the number of neighboring atoms or the reduction of the coordination number, respectively. This may request an rearrangement of atoms at the surface or interface of solids to find a new optimal bonding by lowering the energy. Typical examples are the surface reconstruction exhibited by many semiconductor surfaces rearranging their directional bonds or the formation of carbon nanotubes. A reduction of the coordination number means also that the electrons have less opportunity to hop from site to site and the kinetic energy of the electron or the band width W , respectively, is reduced. Thus, the ratio of the Coulomb interaction U between the electrons on a given site and the band width, U/W , moves toward higher Coulomb interactions, and electron correlation becomes more important and the tendencies towards the appearance of magnetism or a Mott-transition is enhanced. An understanding of these phenomena requires a proper treatment of the electron-electron interaction. Frequently one speaks about one- or two-dimensional solids when the hopping of the electrons are quasi one- or two-dimensional, although the solid crystallizes in a three-dimensional structure. Examples are spin-ladder systems, cubrates, or certain molecular crystals. These systems are out of the scope of this lecture.

1.1 Electrons in a periodic potential: single electron picture

A single electron moving in a periodic potential $V(\mathbf{r}) = V(\mathbf{r} + \mathbf{R}^n)$ provides the foundation of the electronic structure of a crystalline solid. It is described by the single electron Schrödinger equation

$$H_0 \psi_{\mathbf{k}\sigma}(\mathbf{r}) = \left[-\frac{\hbar^2}{2m} \nabla^2 + V_{\text{ion}}(\mathbf{r}) \right] \psi_{\mathbf{k}\sigma}(\mathbf{r}) = \varepsilon_{\mathbf{k}\sigma} \psi_{\mathbf{k}\sigma}(\mathbf{r}), \quad (1)$$

where $\psi_{\mathbf{k}\sigma}$ and $\varepsilon_{\mathbf{k}\sigma}$ are the *Bloch wavefunction* and the band energy, respectively, \mathbf{k} is the electron's lattice momentum, and $\sigma = \uparrow, \downarrow$ is its spin in the S_z direction. \mathbf{R}^n and \mathbf{G}^m with $\mathbf{R}^n \cdot \mathbf{G}^m = 2\pi \mathbf{m} \cdot \mathbf{n}$ are the lattice and the reciprocal lattice vectors, respectively. Here we suppress the band index ν and ignore the spin orbit coupling. According to the *Bloch theorem* the eigensolution of the single electron Schrödinger equation can be expressed in the following general form:

$$\psi_{\mathbf{k}}(\mathbf{r}) = e^{i\mathbf{k}\mathbf{r}} u_{\mathbf{k}}(\mathbf{r}) \quad \text{with} \quad u_{\mathbf{k}}(\mathbf{r}) = u_{\mathbf{k}}(\mathbf{r} + \mathbf{R}^n) \quad (2)$$

where the *Bloch factor* $u_{\mathbf{k}}(\mathbf{r})$ is a periodic function with the same periodicity as the potential. It tells us that the wavefunction of an electron is not periodic,

$$\psi_{\mathbf{k}}(\mathbf{r} + \mathbf{R}^n) = e^{i\mathbf{k}\mathbf{R}^n} \psi_{\mathbf{k}}(\mathbf{r}); \quad (3)$$

but the charge density $|\psi_{\mathbf{k}}(\mathbf{r})|^2$ associated with the state \mathbf{k} is. The *Bloch vectors* are taken from the first *Brillouin zone* (BZ) and are determined by the boundary condition. It is convenient but not necessary to introduce periodic boundary conditions. Assuming that the main region of the crystal has a form of a parallelepiped with sides $N_i \mathbf{a}_i$, $i \in 1, 2, 3$ and imposing the condition

$$\psi_{\mathbf{k}}(\mathbf{r} + N_i \mathbf{a}_i) = \psi_{\mathbf{k}}(\mathbf{r}) \quad \text{for all } i \in 1, 2, 3 \quad (4)$$

we obtain using Eq. 2 these conditions: $\exp(iN_i \mathbf{k} \mathbf{a}_i) = 1$ ($i = 1, 2, 3$) from which we conclude that the Bloch vectors \mathbf{k} take up an infinite discrete set of values which are determined from

$$\mathbf{k} \mathbf{a}_i = \frac{2\pi}{N_i} n_i \quad \text{with } i \in 1, 2, 3, \quad (5)$$

where each n_i is any integer: $n_i = 0, \pm 1, \pm 2, \pm 3, \dots$. For example for a simple cubic lattice one has for any direction i , $k_i = \frac{2\pi}{a} n_i / N_i$. Thus the wave vector \mathbf{k} forms a discrete set in the reciprocal space distributed uniformly within the first BZ. Both the energies $\varepsilon_{\mathbf{k}}$ and the wavefunction $\psi_{\mathbf{k}}(\mathbf{r})$ are some continuous function of \mathbf{k} (we assume that the main region of the crystal is macroscopic and the numbers N_1 , N_2 and N_3 are large). For N_e electrons, in the ground state the lowest N_e states are occupied, and the uppermost energy is called Fermi energy,

$$\max \varepsilon_{\mathbf{k}} = \varepsilon_F. \quad (6)$$

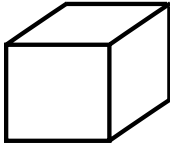
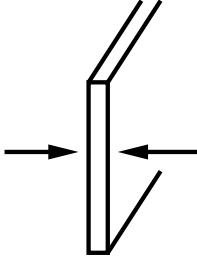
This equation defines the Fermi surface in \mathbf{k} space.

This single electron theory is a very powerful approach in describing the electronic structure of a solid, but it only holds when the Schrödinger equation for N_e electrons can be reduced to a set of single particle Schrödinger equations of the type given in Eq. 1, i.e. only if the N_e -particle Hamiltonian H is a separable sum of single particle Hamiltonians H_0 . Typically the interaction between electrons spoils the separability and makes the N_e -particle Hamiltonian much harder to diagonalize. In many circumstances, much of the Coulomb interaction effects between the electrons can be incorporated into the single particle part of the Hamiltonian by modifying the ion potential V_{ion} to an effective potential V_{eff} , where V_{eff} is a functional of the ground state density $n(\mathbf{r})$. Electrons are then interpreted as quasi-particles with mass m^* instead the undressed electron mass m_0 . The most successful theory of this kind is the density function theory (DFT) which is reviewed by G. Bihlmayer in the lecture A3. If this approximation does not hold the single-particle picture breaks down and the physics is determined by strongly correlated electrons, ignored in this lecture, but treated by E. Koch in lecture A4.

2 Confined Electronic States

In electron confining structures, the basic assumption made in Section 1.1 that the inner part of a solid is macroscopic and that the number of atoms N_i , ($i \in 1, 2, 3$) are arbitrarily large

Table 1: Comparison of the properties of electrons in a two-dimensional electron gas (2DEG) with those in bulk Cu.

	Metal (Cu)	2DEG (GaAs)
		
Electron density	$n = 6 \cdot 10^{22} \text{ cm}^{-3}$	$n = 2 \cdot 10^{11} \text{ cm}^{-2}$
Fermi wave number	$k_F = (3\pi^2 n)^{1/3} = 1.2 \text{ \AA}^{-1}$	$k_F = (2\pi n)^{1/2} = 0.011 \text{ \AA}^{-1}$
Fermi wave length	$\lambda_F \simeq 0.52 \text{ nm} = 5.2 \text{ \AA}$	$\lambda_F \simeq 50 \text{ nm} = 500 \text{ \AA}$
Fermi energy	$E_F = 5 \text{ eV}$	$E_F = 7 \text{ meV}$
Excitation energy	$\Delta E \sim 10^{-10} \text{ eV}$	$\Delta E = 2 \text{ meV}$
Effective mass	$\frac{m^*}{m_o} \sim 1$	$\frac{m^*}{m_o} = 0.067$

does not hold any more, requesting new quantization conditions along the reduced dimension. Since all low energy excitations such electron scattering at impurities, phonons, magnons or transport processes in general taking place in the vicinity of the Fermi surface where occupied states are excited into unoccupied ones, the confinement of carriers within within zero- (0-D), one- (1-D), and two-dimensional (2-D) structures becomes important when the spatial extent of the confining dimension ℓ is of the order of the Fermi wavelength $\lambda_F = 2\pi/k_F$ that depends on the electron density and on the dimensionality. As summarized in Table 2.1, for metals with high free electron concentrations in the 10^{22} cm^{-3} range λ_F is in the order of 0.5 nm (or 5Å), whereas in moderately doped semiconductors with carrier concentrations in the 10^{17} cm^{-3} range, λ_F reaches values of about 50 nm. Both length scales are accessible to modern nanoscience producing wonderful physics by studying the confinement effects.

2.1 Jellium Model

To study the effect of the extent of the system on the character of the eigenfunctions of the electrons and on the distribution on the energy eigenvalues and thus on the macroscopically measurable properties without going into the specific nature of the localization here, we consider an electron in the jellium model, where the underlying periodic structure is homogeneously smeared out and a gas of electrons move in a constant potential which is set to zero without loss of generality. We consider a system which is of macroscopic in D dimensions and confined in $3 - D$ dimensions. We model the confinement on the microscopic length scale ℓ by infinitely

high potential barriers, while in the other directions of macroscopic extent L we use again the periodic boundary conditions.

In the D macroscopic dimensions the corresponding wavefunction (Eq. 2) reduces to just plane waves

$$\psi_{\mathbf{k}}(\mathbf{r}) = \frac{1}{L^{D/2}} e^{i\mathbf{k}\mathbf{r}} \quad \text{and} \quad \varepsilon_{\mathbf{k}} = \frac{\hbar^2}{2m^*} k^2 \quad (7)$$

and the energy eigenvalues change quadratically with the wave vector, whereas D is the number of macroscopic dimensions of the system with the extent $L = N \cdot a$. The \mathbf{k} -values are equidistant and densely spaced due to the macroscopic value of L , $k = \frac{2\pi}{L}n$ with $n \in \mathbf{Z}$. Each state \mathbf{k} is occupied twice, once for spin-up and -down. Then, the largest \mathbf{k} -vector of length $|\mathbf{k}| = k_F$ is determined by the electron density n

$$n = \frac{N_e}{V} = \frac{2}{L^D} \sum_{\mathbf{k}(k < k_F)} 1 = 2 \frac{1}{(2\pi)^D} \int d^D k = 2 \frac{1}{(2\pi)^D} \begin{cases} 2k_F & \text{for } D = 1 \\ \pi k_F^2 & \text{for } D = 2 \\ \frac{4\pi}{3} k_F^3 & \text{for } D = 3 \end{cases} . \quad (8)$$

We can show further that the dimensionality of the electron in the jellium has a strong influence on the form of the density of states $n(\varepsilon)$, a quantity describing the number of states in an energy interval between ε and $\varepsilon + d\varepsilon$. Both the dispersion relation $\varepsilon_{\mathbf{k}} = \frac{\hbar^2}{2m^*} k^2$ and the dimension of the "sphere" enter. We start with density of states in the D -dimensional \mathbf{k} -space per D -dimensional volume element:

$$Z_D d^D k = \frac{1}{L^D} \left(\frac{L}{2\pi} \right)^D [\pi]^{D>1} (2k)^{D-1} dk . \quad (9)$$

The expression $[\pi]^{D>1}$ is equal to 1 for $D = 1$ and π for $D > 1$. The D -dimensional energy spectrum is found, when the dependence of the wavevector is replaced by the energy dependence via the quadratic dispersion relation and a factor 2 for the degree of spin-degeneracy is considered,

$$2Z_D d^D k = 2Z_D(k(\varepsilon)) \frac{dk}{d\varepsilon} d\varepsilon = n_D(\varepsilon) d\varepsilon . \quad (10)$$

Thus one obtains from the D macroscopic dimensions of the system (with $D \geq 1$) a characteristic energy dependence of the spectrum proportional to $\varepsilon^{(D/2)-1}$:

$$n_D(\varepsilon) d\varepsilon = [\pi]^{D>1} \frac{1}{2} \left[2 \frac{\sqrt{2m^*}}{\hbar} \right]^D \varepsilon^{\frac{D}{2}-1} d\varepsilon \propto \begin{cases} \delta(\varepsilon) & \text{for } D = 0 \\ \frac{1}{\sqrt{\varepsilon}} & \text{for } D = 1 \\ \Theta(\varepsilon) & \text{for } D = 2 \\ \sqrt{\varepsilon} & \text{for } D = 3 \end{cases} . \quad (11)$$

We observe that the reduced macroscopic dimensionality of the electron jellium has a strong influence on the form of the density of states. This has important consequences on the electronic properties of confined structures.

In the $3 - D$ directions the system is of microscopic extent ℓ , so that quantization effects become important. As said above we model the confinement by infinitely high potential wells. These potential barriers enforce new boundary conditions for the wave functions. The infinite potential

well is equivalent to vanishing wave functions at the boundary with standing wave solutions. For convenience we focus first on quantum films, i.e. $D = 2$. The boundary condition, e.g. along x -direction $\psi(x = 0) = \psi(x = \ell) = 0$ results then in the eigenfunction

$$\psi_{m,k_y,k_z} = \sqrt{\frac{2}{\ell}} \sin\left(\frac{m\pi}{\ell}x\right) \frac{1}{L} e^{i(k_y y + k_z z)} \quad (12)$$

with the eigenvalue spectrum

$$\varepsilon_{m,k_y,k_z} = \varepsilon_m + \varepsilon_{k_y,k_z} \quad \text{where} \quad \varepsilon_m = \frac{\hbar^2}{2m_\ell} \frac{m^2 \pi^2}{\ell^2} \quad \text{and} \quad \varepsilon_{k_y,k_z} = \frac{\hbar^2}{2m^*} (k_y^2 + k_z^2) \quad (13)$$

While the spectrum of ε_{k_y,k_z} is quasi continuous because of the macroscopic dimension L , the spectrum of ε_m is truly discrete because ℓ is microscopic. (We also assume two different effective masses m^* and m_ℓ). The wavenumber for the different wavefunctions in x -direction differ by $\delta k = \pi/\ell$. This is a large value due to the microscopic value of ℓ . Thus the energy eigenvalues for different m lie far apart. One obtains e.g. in x -direction discrete energy values separated by

$$\delta E_m = E_m - E_{m-1} = \frac{\hbar^2}{2m_\ell} \frac{\pi^2}{\ell^2} (2m - 1) \gg k_B T. \quad (14)$$

Strictly speaking, this applies to an infinitely deep potential well. However, we can still use the same equation as long as E_m is in the vicinity of the bottom or the top of a band. For the quantization to be important, the difference between the levels should be much larger than the thermal energy $k_B T$. Using this condition, we find, for example, that in GaAs where $m_\ell/m_o = 0.067$, the levels are quantized at room temperature when $\ell = 15$ nm. In order to exhibit two-dimensional behavior there should be only one single level within $\pm k_B T$ of the Fermi level. Several levels within the Fermi cut-off would already approach a three-dimensional continuum. Similarly we can derive the results of 1-D and 0-D case. For example, the wavefunction of a one-dimensional wire is then give by:

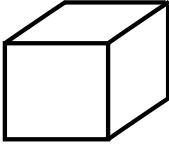
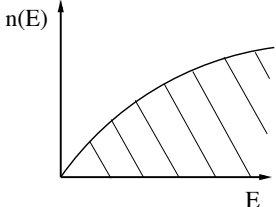
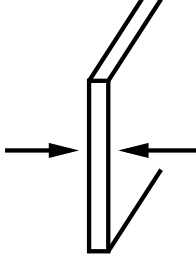
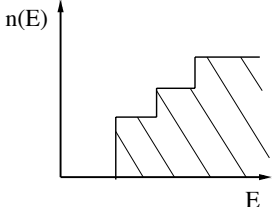
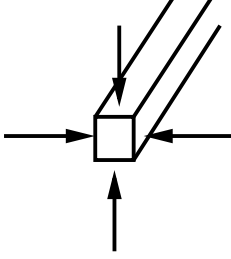
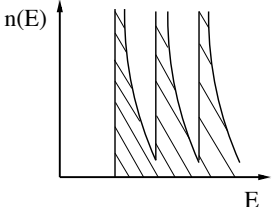
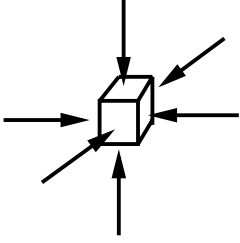
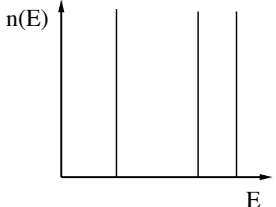
$$\psi_{m,n,k_z} = \frac{2}{\ell} \sin\left(\frac{m\pi}{\ell}x\right) \sin\left(\frac{n\pi}{\ell}y\right) \frac{1}{\sqrt{L}} e^{ik_z z}. \quad (15)$$

Further results are compiled in Table. 2.1 together with the density of states.

2.2 Quantum-Well States

Quantum-well states – quantized electronic states confined within a thin slab can be prepared in nature. They are well-known in systems containing semiconductors and insulators such as the InP-In_xGa_xAs family. Semiconductor quantum wells support these states near the edges of the fundamental gap where the band-gap mismatch leads to electron confinement. Such states play an important role in the operation of many optoelectronic devices (e.g. the “quantum-well” laser). In general, the question of electron reflection characteristic of the potential well at which the electron is scattered versus the transmission characteristic of the leakage of electrons depends on the “electronic mismatch” or the band-structure mismatch of materials. The electron

Table 2: Extended systems in $D = 3, 2, 1, 0$ dimensions, illustration of the density of states $n(\varepsilon)$, eigenfunctions $\psi(\mathbf{r})$, $\psi_{m,\mathbf{k}_{\parallel}}(\mathbf{r})$, $\psi_{m,n,k_y}(\mathbf{r})$, and $\psi_{m,n,l}(\mathbf{r})$, as well as the expression for the density of states. The summation runs over the discrete eigenvalue spectra.

 <p style="text-align: center;">BULK</p> 	 <p style="text-align: center;">QUANTUM FILM</p> 	 <p style="text-align: center;">QUANTUM WIRE</p> 	 <p style="text-align: center;">QUANTUM BOX</p> 
$\psi_{\mathbf{k}}(\mathbf{r}) = \frac{e^{i\mathbf{k}\mathbf{r}}}{\sqrt{V}}$ $\varepsilon(\mathbf{k}) = \frac{\hbar^2}{2m^*}(k_x^2 + k_y^2 + k_z^2)$ $n(\varepsilon) = a^{(3)}\sqrt{\varepsilon}$	$= \phi_m(x) \frac{e^{i(k_y y + k_z z)}}{\sqrt{A}}$ $\varepsilon_m(\mathbf{k}_{\parallel}) = \varepsilon_m + \frac{\hbar^2}{2m^*}(k_x^2 + k_y^2)$ $= \sum a_m^{(2)} \Theta(\varepsilon - \varepsilon_m)$	$= \phi_m(x) \phi_n(y) \frac{e^{ik_z z}}{\sqrt{L}}$ $\varepsilon_{m,n}(k_y) = \varepsilon_m + \varepsilon_n + \frac{\hbar^2}{2m^*} k_y^2$ $= \sum a_{m,n}^{(1)} \frac{1}{\sqrt{\varepsilon - \varepsilon_m - \varepsilon_n}}$	$= \phi_m(x) \phi_n(y) \chi_l(z)$ $\varepsilon_{m,n,l} = \varepsilon_m + \varepsilon_n + \varepsilon_l$ $= \sum_{m,n,l} \delta(\varepsilon - \varepsilon_{m,n,l})$

dynamics is determined by the energy, the crystal momentum conservation and the symmetry match of the propagating electrons. Thus, even without an absolute gap, electron confinement is still possible near the edge of a “relative” gap. An this holds also for metal-on-metal systems such as Ag(111) on Au(111) [1] or Co on Cu(100) [2] to name two well-known ones.

Quantum-well states can be well-understood on the basis of the bulk band structure. We exemplify this for Cu(100) films of finite thickness embedded in vacuum. In Fig. 1(left) we find the band-structure $\varepsilon_{\mathbf{k}}$ of bulk Cu along high-symmetry lines. For a film of finite thickness oriented along the (100) direction the translational symmetry is broken along Γ -X direction, the \mathbf{k} -values along this Δ line are not anymore arbitrarily dense but are quantized according to the number of layers N in the (100) direction, $k_{\perp} = \frac{m}{N} \frac{\pi}{a}$. In good approximation one can derive the eigenvalue spectrum for the thin films writing $\varepsilon_{\mathbf{k}} = \varepsilon_{k_{\perp}, \mathbf{k}_{\parallel}}$, with $\mathbf{k}_{\parallel} \in 2\text{DBZ}$ (two-dimensional

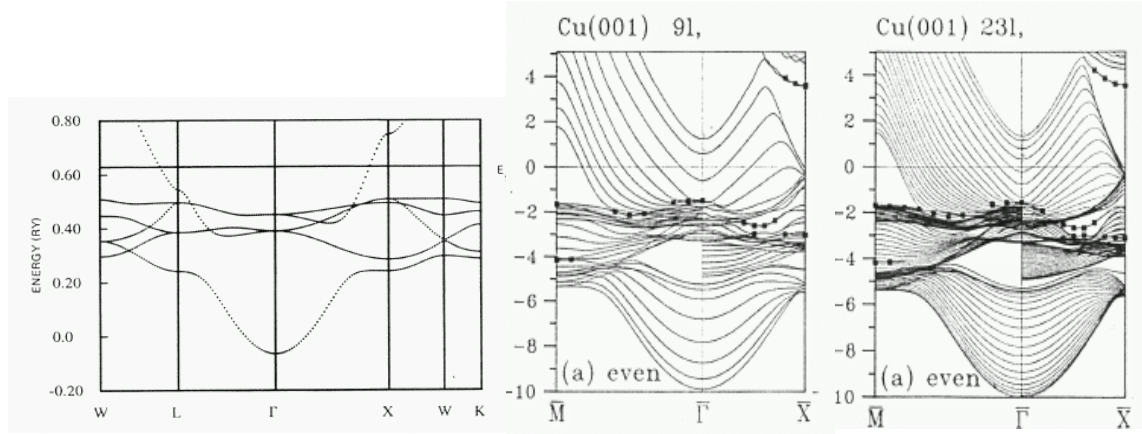


Fig. 1: (left): Bandstructure of fcc Cu, (middle): band structure of a fcc Cu film of 9 ML thickness in vacuum, (right): respective film of 23 ML thickness.

Brillouin zone). States between Γ -X map onto the $\bar{\Gamma}$ -point. In the ideal case of a of an isolated film composed of n layers, the finite size of the system imposes a quantization of the levels, so that n discrete levels $\varepsilon_n(\mathbf{k}_{\parallel})$ are created for every two-dimensional vector k_{\parallel} . The energy level spectrum changes with the film thickness as calculated for Cu(001) and shown in Fig. /reffig:Cu100-BS-23ML in analogy with Eq. 14 of an electron in a box. The number of allowed states increases with the film thickness while their energy separation decreases. The electronic structure converges to that of bulk Cu with increasing film thickness. At the Fermi surface $2\pi/(k_{\text{BZ}} - k_{\text{F}}) \approx 6$ atomic layers. Therefore, when the thickness of the film is increased by about 6 layers an additional state moves through the Fermi energy.

The term quantum-well states is well chosen. This is shown in Fig. 2(left) by counting the number of s electrons in a sphere around an atom across the 23 layers of a Cu film for the three lowest quantum-well states at the $\bar{\Gamma}$ point together with the theoretical solution for a potential well with infinite walls. The agreement is striking.

With photoemission the electronic structure of the film can be probed as a function of binding energy, wave vector \mathbf{k}_{\parallel} , spin and film thickness. In practice, the complexity (i.e. roughness, interdiffusion, clustering) of the film growth mode often makes the observation of the quantization effects difficult or even impossible. However, there are favorable cases in which the film grows almost perfectly layer by layer, the formation of “quantum-well states” can be directly observed in the photoemission spectra. As an example Fig. 2(right) shows the photoemission spectra of thin Cu films epitaxially grown on fcc-Co(100) [2]. In the geometry of this measurement the photoemission probes the electronic structure of Δ_1 symmetry at the wave vector $\mathbf{k}_{\parallel} = \bar{\Gamma}$. The spectra of the films show several structures derived from the Cu electronic states, with binding energies varying with film thickness. The quantization effects on these levels is visible in these spectra up to a thickness of 50 atomic layers. The quantum-well condition is only fully filled for minority states but not for majority states, therefore the quantum well states are spin-polarized.

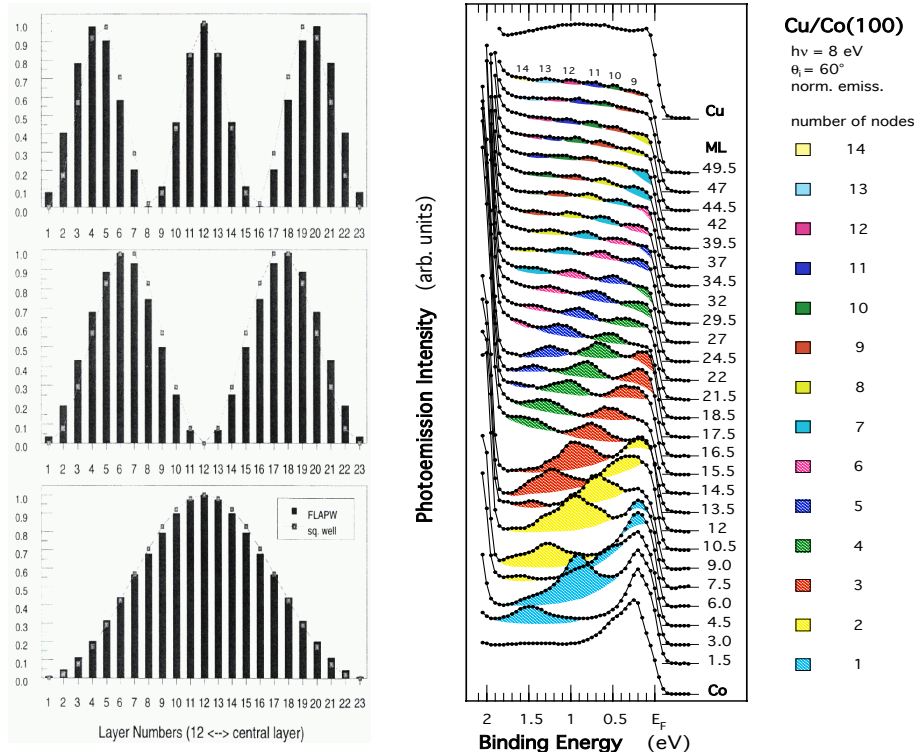


Fig. 2: (left): Number of s electrons in a sphere around an atom across the 23 layers of a Cu film for the three lowest quantum-well states at the $\bar{\Gamma}$ point together with the theoretical solution for a potential well with infinite walls. (right): Photoemission spectra of ultrathin Cu films on fcc-Co(100). The shaded spectral structures with bonding energy depending on the film thickness, derive from the quantization of the energy levels due to electron confinement. They are observed up to 50 atomic layers, (90Å), thickness [2].

3 Electronic Structure of Surfaces

In Section 2 we discussed the occurrence of electron confinement assuming infinite potential wells. For most cases this is a simplification. In reality, we deal with finite and gradually changing potentials either toward a vacuum or an interface of a different material. This leads to new boundary conditions and surfaces and interfaces induce new electronic states which do not exist in the bulk crystal. These *surface states*, *interface states* or *surface resonances*¹ are to be discussed here briefly first for the 1-D case. Then we present well-investigated examples of metal surfaces, of the surface of the semi-metal Bi, whose surface becomes metallic and of some semi-conductor surfaces. Most metal have delocalized electrons and the generation of a surface changes very little the atomic positions in the vicinity of the surfaces. Therefore most metal surface remain structurally ideal surfaces. This is quite different to semiconductor surfaces, with half-filled directional lone-pair bonds, whose atoms rearrange in order to saturate these bonds. Surface states of metals are believed to play an important role in catalysis, but also in surface diffusion, the interaction of atoms across the surface and correlations effects such as

¹Surface resonances are states, which have a high probability density at the surface, but couple to bulk states.

the Kondo effect of magnetic adatoms on nonmagnetic metal surfaces. Semiconductor interface states can be electronically active and may influence the electrostatics in semiconductor devices.

3.1 Qualitative Discussion in One Dimension

The surface system consists of the two infinitely extended semi-infinite spaces, the vacuum ($-\infty < z < 0$) and the bulk crystal ($0 \leq z < \infty$).

The system is described by the Schrödinger equation:

$$\left[-\frac{\hbar^2}{2m} \frac{d^2}{dz^2} + V(z) \right] \psi_\nu(z) = \varepsilon_\nu \psi_\nu(z). \quad (16)$$

Before we solve the Schrödinger equation for this system, we recall the solution of the Schrödinger equation for the two reference systems: bulk crystal and vacuum.

The Bulk Crystal

In the bulk crystal, the effective potential of the electrons is lattice periodic, i.e.

$$V(z + a) = V(z), \quad (17)$$

whereby a is the 1-D lattice constant. The lattice-periodic translation symmetry induces the Bloch vector k as quantum number. The range of values of k lies within the 1st BZ, and the eigensolutions to this potential have Bloch symmetry:

$$\psi_{k\nu}(z + a) = e^{ika} \psi_{k\nu}(z) = e^{ik(z+a)} u_{k\nu}(z), \quad (18)$$

whereas $u_{k\nu}(z)$ is the lattice periodic Bloch factor as introduced in the Introduction, i.e. $u_{k\nu}(z) = u_{k\nu}(z + a)$. $\varepsilon_{k\nu}$ is the *band structure* of the periodic crystal. ν labels the bands. For reasons of wavefunction normalizability only real values of k ($k \in \mathbf{R}$) are allowed.

The Vacuum

Setting the potential $V(z) = 0$, we obtain for Schrödinger equation in vacuum

$$-\frac{\hbar^2}{2m} \frac{d^2}{dz^2} \phi_K(z) = \varepsilon_K \phi_K(z) \quad (19)$$

with the solution

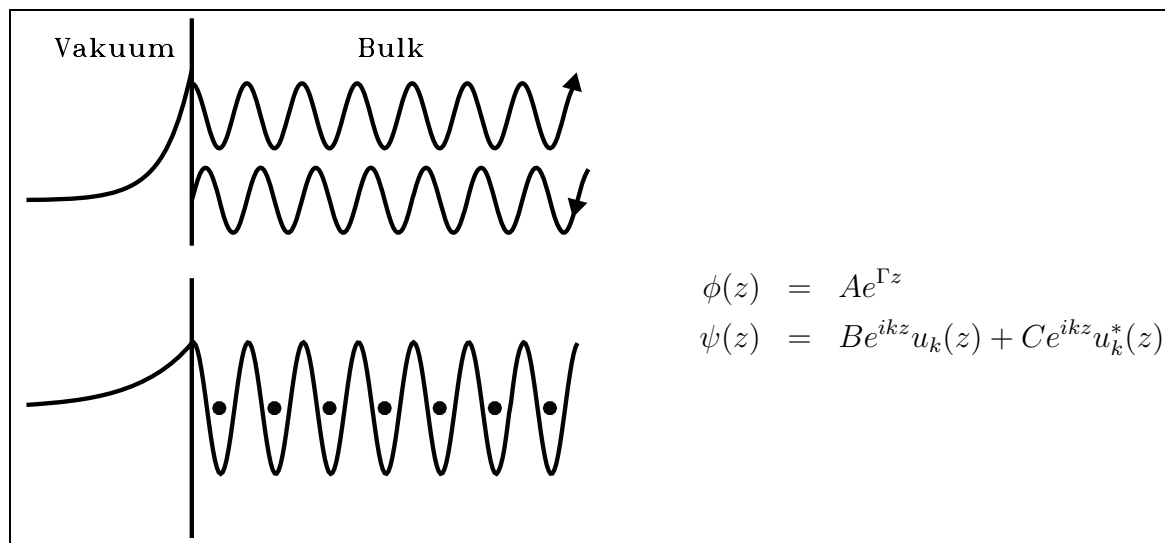
$$\phi_K(z) = \frac{1}{\sqrt{L}} e^{iKz} \quad \text{and} \quad \varepsilon_K = \frac{\hbar^2}{2m} K^2 \quad \text{or} \quad K = \pm \sqrt{\frac{2m}{\hbar^2} \varepsilon_K}. \quad (20)$$

L is a macroscopic normalization length. If $\varepsilon \geq 0$, then K is real, if $\varepsilon < 0$, then K takes imaginary values. This solution is mathematically possible, must be rejected however for physical reasons, since this solution is not normalizable, because of the divergence for $z \rightarrow \pm\infty$.

The Surface

For the surface system one deals with both semi-infinite half-spaces, the vacuum and the bulk. However, with respect to the periodic bulk system, the boundary conditions for the normalization of the wave function change. Now, also solutions with complex $Q = K + i\Gamma$ or $q = k + i\gamma$ can be induced, which had to be excluded before. We discuss this briefly for energies of bound electrons $\varepsilon < 0$. Thereby, there are two different possibilities:

1.) Energy $\varepsilon < 0$ is placed within a band² of the bulk crystal:



There are incoming and outgoing crystal states, which are elastically reflected at the surface. Their amplitudes drop exponentially into the vacuum. The three constants are determined by two boundary conditions at the surface ($z = 0$)

$$(i) \quad \phi(0) = \psi(0), \quad \text{and} \quad (ii) \quad \left. \frac{d\phi}{dz} \right|_{z=0} = \left. \frac{d\psi}{dz} \right|_{z=0}, \quad (21)$$

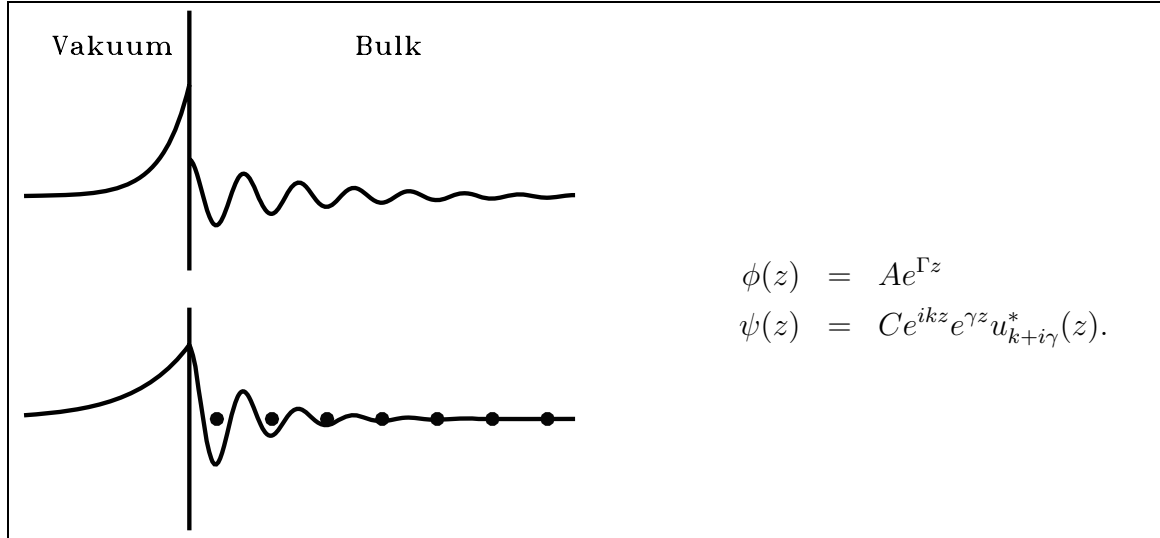
and (iii) the normalizability. These three conditions can always be satisfied and therefore there are solutions for all energies within a band.

2.) Energy $\varepsilon < 0$ is located in a band gap³ of the bulk crystal:

There are no current carrying states, neither in the vacuum nor in the crystal. Therefore, only solutions are permitted with wavefunctions fading exponentially into the vacuum and bulk, which are described by means of complex Q and q . Normalizability together with the demand for a continuous differentiable adjustment of both wave function at the surface leads to an eigenvalue problem for a bound state, the surface state with the energy ε_s . The localization $\gamma(\varepsilon)$ and $\Gamma(\varepsilon)$ is largest in the center of the gap and changes at the band edge continuously into

²permitted eigenvalue spectrum ε_k .

³No permitted eigenstates. It occurs in semiconductors and insulators but also in metals. With the latters, however, only within limited areas of the Brillouin zone, so-called partial gaps and pockets.



the bulk band. Between the lower and the upper edge of the gap the phase of the wave function changes by π .

3.2 Description in Three Dimensions

Real bulk crystals are three-dimensional, consequently the Bloch vectors \mathbf{k} and the Brillouin zone are three-dimensional vectors and objects, respectively.

The surface breaks in one direction the lattice-periodic translation symmetry, and the three-dimensional lattice-periodic translation symmetry reduces to two directions parallel to the surface. The unit cell for the atoms is semi-infinite in direction normal to the surface. This leads to a symmetry reduction of the underlying crystal lattice. For example, cubic crystals with a surface are described in terms of a tetragonal unit cell. Due to the symmetry lowering, the 3-D Bloch vector $\mathbf{k} = (k_{\perp}, \mathbf{k}_{\parallel})$ is not a good quantum number anymore, and only the two-dimensional parallel component \mathbf{k}_{\parallel} remains a good quantum number. Thus, the electronic states are just described by 2-D Bloch vectors \mathbf{k}_{\parallel} and by 2-D Brillouin zones, also called surface Brillouin zones (SBZ).

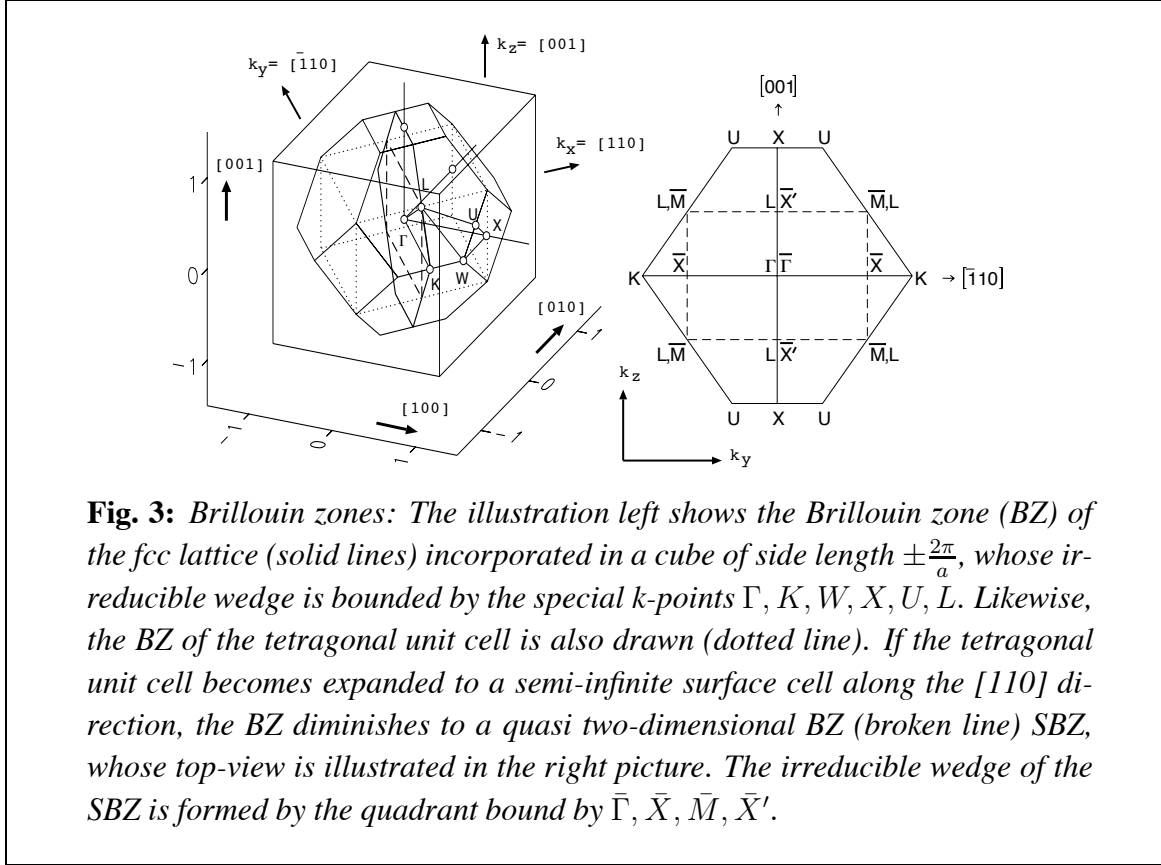
For example, the wavefunction in the vacuum can be expressed in terms of the Bloch representation,

$$\psi_{\mathbf{k}_{\parallel}\nu}(\mathbf{r}_{\parallel}, z) = e^{i\mathbf{k}_{\parallel}\mathbf{r}_{\parallel}} u_{\mathbf{k}_{\parallel}\nu}(\mathbf{r}_{\parallel}, z). \quad (22)$$

Due to the 2-D lattice periodicity of the Bloch factors $u_{\mathbf{k}_{\parallel}\nu}(\mathbf{r}_{\parallel}, z)$, $u_{\mathbf{k}_{\parallel}\nu}(\mathbf{r}_{\parallel}, z) = u_{\mathbf{k}_{\parallel}\nu}(\mathbf{r}_{\parallel} + \mathbf{R}_{\parallel}, z)$, it is possible to expand $u_{\mathbf{k}_{\parallel}\nu}(\mathbf{r}_{\parallel}, z)$ in terms of a 2-D Fourier series and the wave function in the vacuum can be expressed as

$$\psi_{\mathbf{k}_{\parallel}\nu}(\mathbf{r}_{\parallel}, z) = \sum_n c_{\mathbf{k}_{\parallel}\nu}^n d_{\mathbf{k}_{\parallel}}^n(z) e^{i(\mathbf{k}_{\parallel} + \mathbf{G}_{\parallel}^n)\mathbf{r}_{\parallel}}. \quad (23)$$

$\exp(i\mathbf{G}_{\parallel}^n \mathbf{r}_{\parallel})$ are the 2-D plane waves parallel to the surface and $d_{\mathbf{k}_{\parallel}}^n(z)$ are the one-dimensional z -dependent basis function, which describe the decay into the vacuum, and which can be deter-



mined by solving a 1-D Schrödinger equation in the vacuum

$$\left[-\frac{\hbar^2}{2m} \frac{d^2}{dz^2} + V(z) - \varepsilon_v + \frac{\hbar^2}{2m} (\mathbf{k}_{\parallel} + \mathbf{G}_{\parallel}^n)^2 \right] d_{\mathbf{k}_{\parallel}}^n(\varepsilon_v, z) = 0. \quad (24)$$

for a laterally averaged potential $V(z)$ for a reference energy ε_v .

3.3 Metallic Surfaces

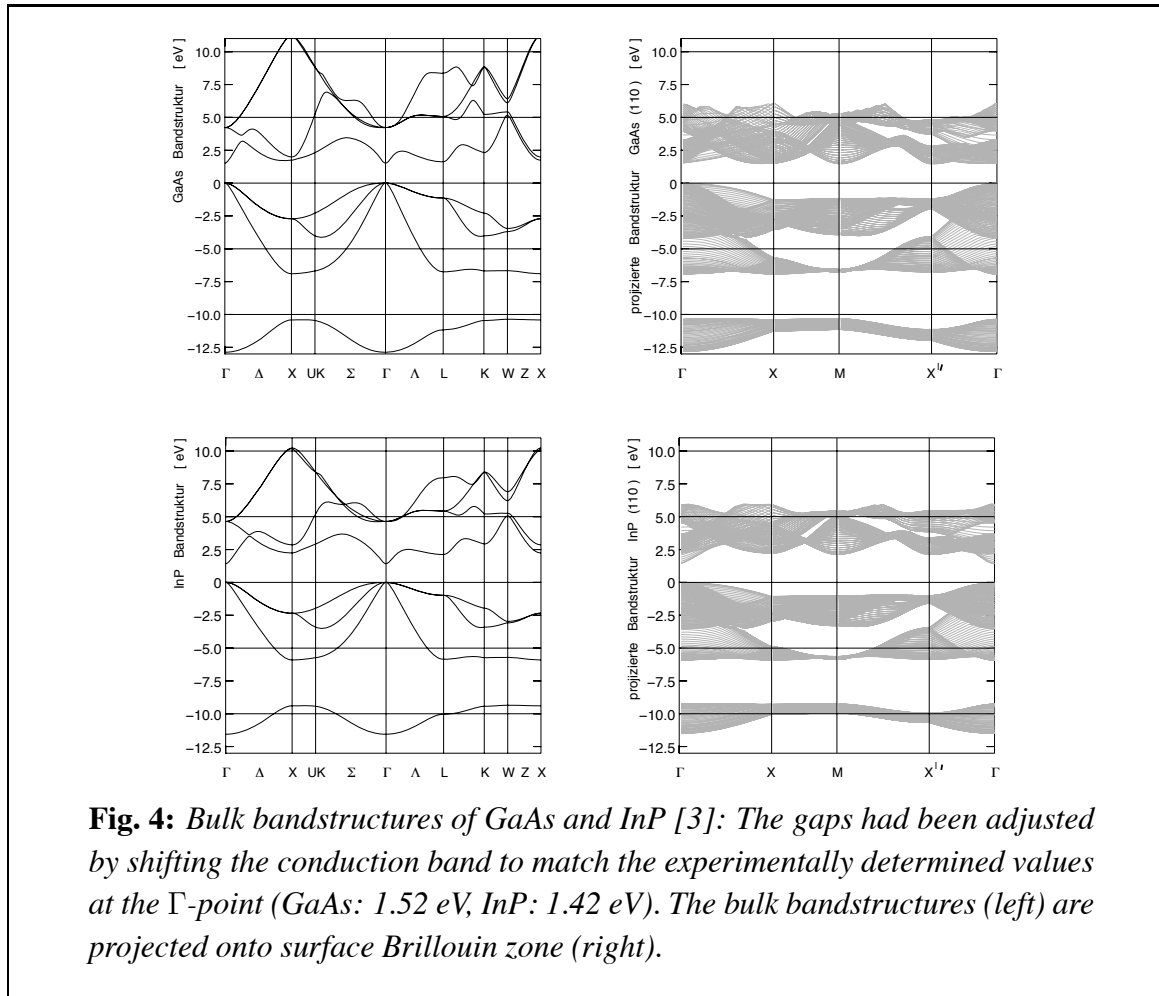
An ideal surface is obtained cutting through the crystal by means of an infinite two-dimensional plane along crystal planes. A first conception of the bandstructure of the semi-infinite space is obtained by projecting the three-dimensional bandstructure on the two-dimensional surface Brillouin zone, thus

$$\varepsilon_{\mathbf{k}\nu} = \varepsilon_{(\mathbf{k}_{\parallel}, k_{\perp})\nu} =: \varepsilon_{\mathbf{k}_{\parallel}}^{PBS}(k_{\perp}\nu). \quad (25)$$

The resulting bandstructure is also called *projected bulk bandstructure*, abbreviated as PBS. This projection is demonstrated in Fig. 3.

By view of Fig. 3 it becomes obvious that in the case of the (110)-surface all states of k_{\perp} along Σ (i.e. between Γ and K) contribute to the two-dimensional k_{\perp} -point $\bar{\Gamma}$. Figure Fig. 4 shows for examples the so evaluated PBS of the GaAs(110) and InP(110) surfaces Band gaps in the

bulk bandstructure produce also gaps in the PBS. Additionally, so-called pockets arise in certain k_{\parallel} -directions and for certain k_{\parallel} -values, in which no Bloch waves can exist just as little as in the gaps. It is obvious that there are different PBS for different surface geometry.



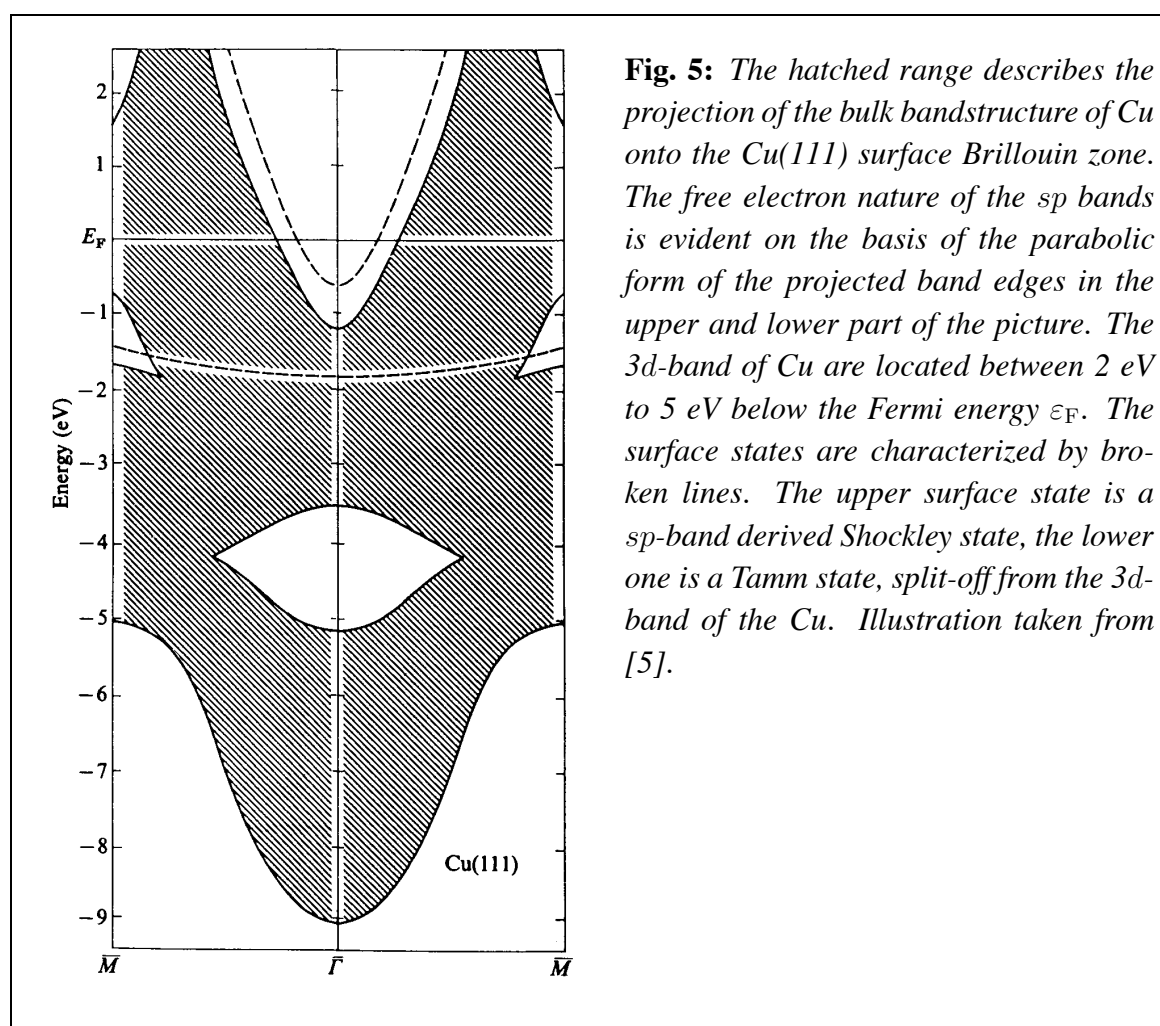
Surface states and -resonances are additional solutions, which cannot be derived from the bulk bandstructure. For historical reasons one calls the surface states, which can be described well in the model of free electrons, Shockley states [6], and those, which can be described well in the model of tightly bound states (*tight binding model*), Tamm states [7]. For real surface states, both concepts apply only approximately. Generally the delocalized s - and p -electrons of metals, d -orbital of lanthanides and actinides are well described by Shockley states, while the Tamm concept applies to p electrons of some semiconductors, d -orbitals of transition metals and f -orbitals of actinides. There are surface states at nearly all surfaces.

So far we assumed that at surfaces atomic positions do not change. This is never completely fulfilled in nature, since the bonding conditions change drastically in the surface due to the absence of neighboring atoms. The positions of the atoms in a real surface can deviate from the ideal bulk terminated surface by either a *surface relaxation* or by a *surface reconstruction*. In the case of the relaxation, the surface unit cell agrees with that of the ideally terminated one, but the

atomic positions are shifted along symmetry conserving degrees of freedom (e.g. the surface-normal). Symmetry lowering does not take place. In the case of the surface reconstruction an additional change of the translation symmetry parallel to the surface occurs.

Many low-index surfaces of metals (e.g. (100), (110) or (111)) typically do not reconstruct (exceptions e.g.: Au(111), Ir(100), Ir(110), Au(110), Rh(110)) and relax little. Here the model of the ideal surface works rather well.

The Cu(111) Surface



The noble metals crystallize in the fcc crystal structure. Their projected bulk band structures exhibit a large band gap around the L-point of the fcc Brillouin zone (see Fig. 3). In fact, noble metal (111) surfaces have both a Shockley [8] and a Tamm state [9]. Both states have textbook character and were intensively studied by photoemission and inverse photoemission. The Shockley state has a parabolic dispersion, and the electrons of this state behave nearly like free electrons. It is directly located at the Fermi energy and is thereby easily accessible to spectroscopy with the scanning tunneling microscope (STM) or photoemission. As example

we show the surface bandstructure of Cu(111). Results for Ag(111) and Au(111) are found for example in Ref. [10].

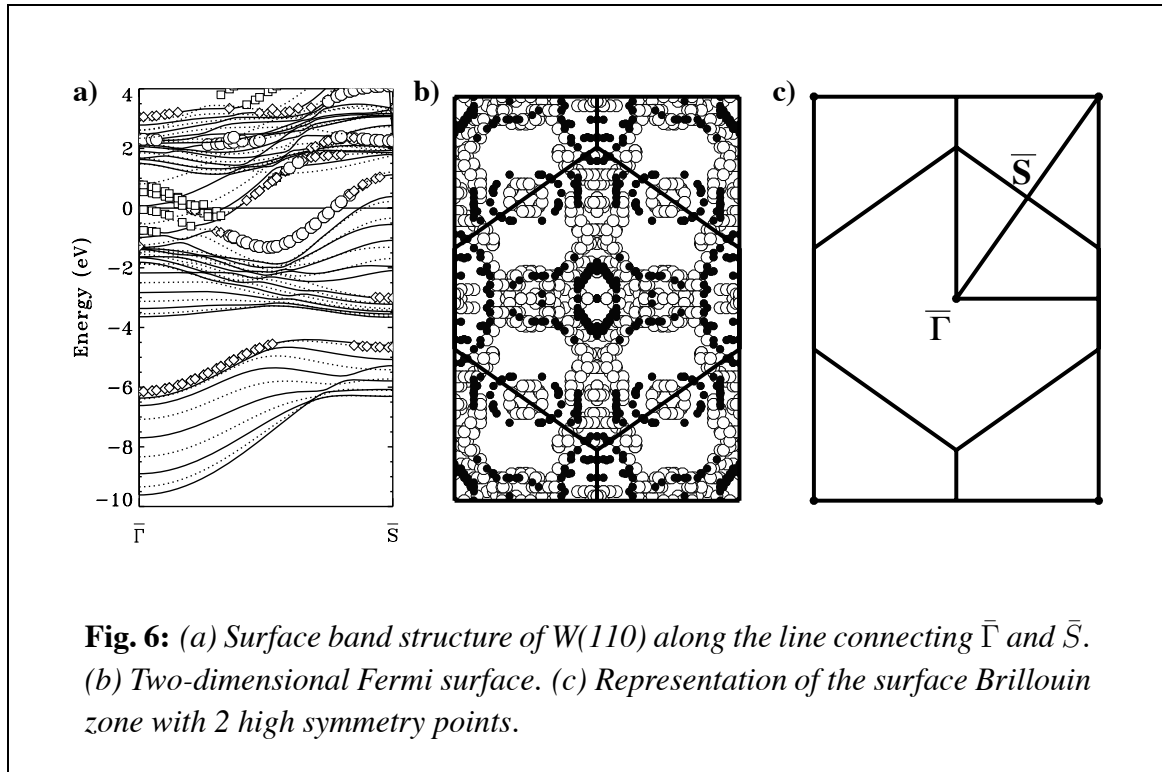
Table 3: Summary of experimental results fitted to a parabola after Reinert et al. [11]. The two parabolas of the Au(111) surface states are centered at $\pm 0.013 \text{ \AA}^{-1}$.

	$\varepsilon_0[\text{meV}]$	m^*/m_o	$k_F[\text{\AA}^{-1}]$	$\lambda_F[\text{\AA}]$
Cu	435 ± 1	0.412	0.215	29.2
Ag	63 ± 1	0.397	0.080	78.5
Au	487 ± 1	0.255	0.167/0.192	37.6/32.7

In Table 3 we summarize the maximum binding energy ε_0 at (or close to) the $\bar{\Gamma}$ -point, the effective mass relative to the electron mass m_o , the Fermi wavevector k_F and Fermi wavelength λ_F of the surface state for the (111) surfaces of the three noble metals. These surface states became a play ground for studying electron confinement and the consequences for symmetry lowering at surfaces. For instance, the binding energy of the Ag(111) surface state is smallest. That implies, that also the PBS has the smallest gap of all three metals. Ag and Au have nearly the same lattice constant and Ag can be grown on Au and vice versa. Since the PBS of Au exhibits a larger gap than Ag, there is an energy range of nearly 1 eV where Ag *sp* states of Ag films grown on Au(111) bounce against the Au gap and are partially reflected leading to quantum-well states, the first quantum-well states exhibited in metals, at least to my knowledge (see Ref. [1]). No quantum-well states will be found for Au films on Ag(111) substrates as here no gap appears. The surface state will remain in both cases. Depending on the thickness the latter will continue as an interface state into the substrate. The lateral confinement of this two-dimensional surface state by artificially made quantum corrals of the size of the wavelength λ_F e.g. by atom manipulation or due to the presence of step edges leads to interesting electronic effects observable with the scanning tunneling microscope.

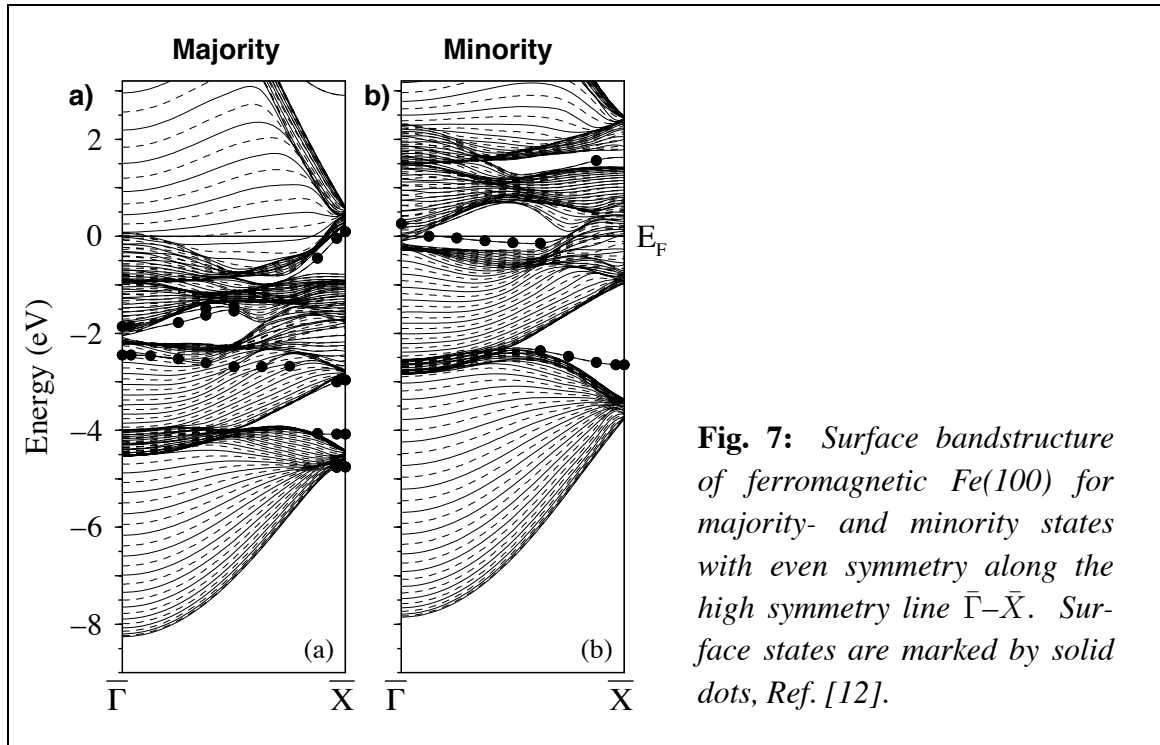
The W(110) Surface

W(110) is a further very intensively examined surface [23]. W crystallizes in the bcc structure and the (110) oriented is the most compact one with densely packed centered-rectangular layers. Fig. 6a shows the band structure from $\bar{\Gamma}$ to \bar{S} of a W(110) slab of finite thickness. Increasing thickness would fill in more discrete bands into an energy regime which is identified as the PBS. In addition to these states we identify the surface band (open dots) which is split-off from the bulk *d* band and has likewise *d* character. This surface band cuts the Fermi energy near the zone boundary. For comparison Fig. 6b shows the two-dimensional Fermi surface of W(110) with all those states added whose wave function leak out of the surface. Open dots are bulk states, solid dots are surface states. The fact that the surface band causes the ellipse of surface states at the \bar{S} -point is to be recognized clearly, just as the surface resonance states around $\bar{\Gamma}$.



The Fe(100) Surface

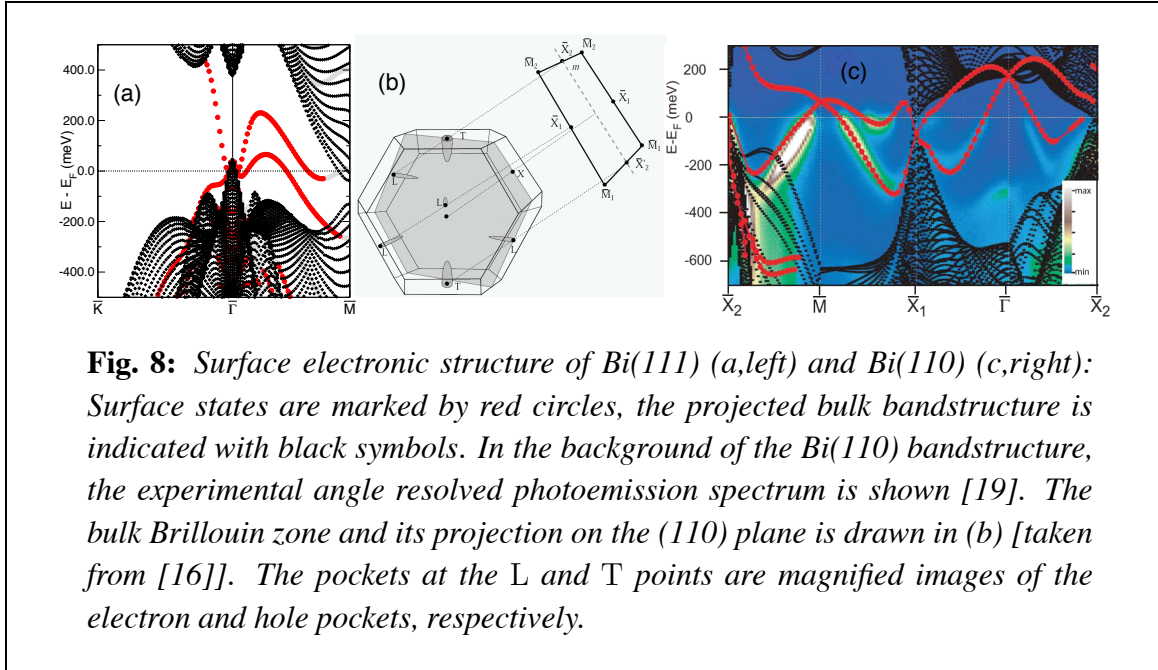
In Fig. 7 we show the surface bandstructure (more accurately, it was a calculation of a 49-layer film, whose bandstructure approaches the one of the semi-infinite system quite well) for even-symmetry states of Fe(100) along the high symmetry line connecting $\bar{\Gamma}$ with \bar{X} . The Fe-surface is magnetic (surface magnetic moment amounts to $2.8 \mu_B$ as compared to the bulk magnetic moment of $2.25 \mu_B$); therefore all states are spin-split into two spin directions of S_z , which we classify here as majority and minority states. Along the high-symmetry line between $\bar{\Gamma}$ and \bar{X} one finds surface state bands, whose energy at the $\bar{\Gamma}$ point is around 0.4 eV for the minority surface state and around -2.0 eV for the majority one. A close look at Fig. 7 reveals that the surface state band $\bar{\Gamma}-\bar{X}$ penetrates at the $\bar{\Gamma}$ point into the bulk band and changes its character to a surface resonance. Obviously, with this $d_{3z^2-r^2}$ state at $\bar{\Gamma}$ we have a surface state (or resonance) at hand, whose properties depend on the magnetism, chemical environment, lattice distortion, the surface morphology, the alloy formation and so on. Thus, the spectroscopic investigation of this state permits information on the local chemistry as in the the investigations of the systems Cr, Fe(100) [12], the alloy formation of Cr/Fe(100) [13] or the investigation of one-dimensional domain boundaries of the two-dimensional surface alloy Fe(100) c(2 × 2) Si [14].



The Bi Surfaces

In metals, the formation of a surface may lead to the appearance of a surface state in the gaps of the projected bulk bandstructure. But normally, these state occupy only a small fraction of reciprocal space and their contribution to the total density of states is small. Therefore, surface states will have just a small effect on the overall electronic properties of metals. On the other hand, surface formation in semiconductors leads to a massive breaking of covalent bonds, and consequently a fundamental rearrangement of charges. To avoid the excessive formation of surface states, these surfaces often reconstruct to saturate their dangling bonds. Semimetallic systems, i.e. substances which have no bandgap but vanishing or almost zero density of states at the Fermi level form an intermediate class. Bismuth, for example, is a semimetal that shows large projected bandgaps at the Fermi level for all surfaces. Here, we discuss low-index surfaces, that do not reconstruct but show prominent surface states which significantly alter the electronic properties of these surfaces.

Bi has a rhombohedral structure, that can be imagined to result from a small distortion of two penetrating face-centered cubic (fcc) lattices along the body-diagonal forming a two-atomic lattice with a basis vectors $(\pm u, \pm u, \pm u)$ where u is slightly smaller than $1/4$. Like in the case of the Cu(111) surface, the Bi(111) surface thus consists of densely packed hexagonal layers, which are – in contrast to the fcc lattice – not evenly spaced, but form relatively stable bilayer structures [15]. The projected bulk-bandstructure of the Bi(111) surface is shown on the left of Fig. 8. Only at the $\bar{\Gamma}$ and \bar{M} points small Fermi surfaces are formed, originating from the L and T points of the bulk Brillouin zone (Fig. 8(b)). Along the line $\bar{K}\bar{T}\bar{M}$ there is a large projected



bulk bandgap extending throughout the whole Brillouin zone. In this bandgap two states appear, that change the character of the surface from semiconducting to metallic. As it turns out, these two states are actually spin-split partners of a single surface state [17]. This spin-splitting can arise on a nonmagnetic surface due to the Rashba spin-orbit splitting, a relativistic effect which gets particularly strong for materials with high nuclear number [18]. It is a consequence of the lowering of symmetry at the surface, in particular the loss of structural inversion symmetry. Therefore, this spin-orbit splitting should in principle affect all surface states, but actually the effect is often too small to be observed.

Each Bi atom has three nearest neighbors and quasi-covalent bonds connect these neighbors. On the (111) surface, no bond-breaking occurs and surface states appear only in certain directions in the Brillouin zone. On other low-index surfaces, e.g. Bi(110), one of these bonds is broken and a “surface state band” extending through the full, rectangular Brillouin zone appears (right of Fig. 8). Again, spin-orbit coupling effects cause a spin-splitting of the surface state. Despite the fact, that one out of three nearest-neighbor bonds is broken on this surface, there is no reconstruction observed on Bi(110) [20]. A similar situation is encountered on the quasihexagonal Bi(100) surface, where again a nearest-neighbor bond is broken and a surface state extends through the whole Brillouin zone [21].

3.4 Semiconductor Surfaces

The III-V (110) Surface

Example semiconductor surfaces exhibiting surface relaxations are the (110) surfaces of the III-V compound semiconductors (e.g. GaAs(110) or InP(110)). All show the same structure

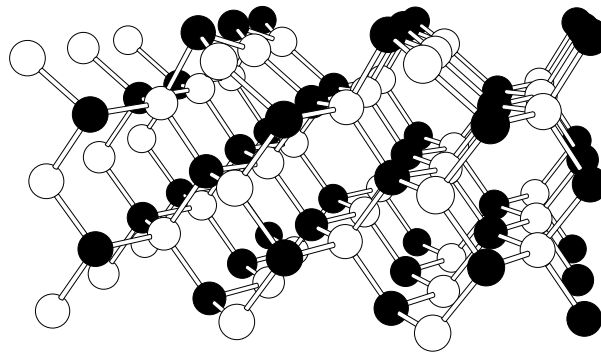


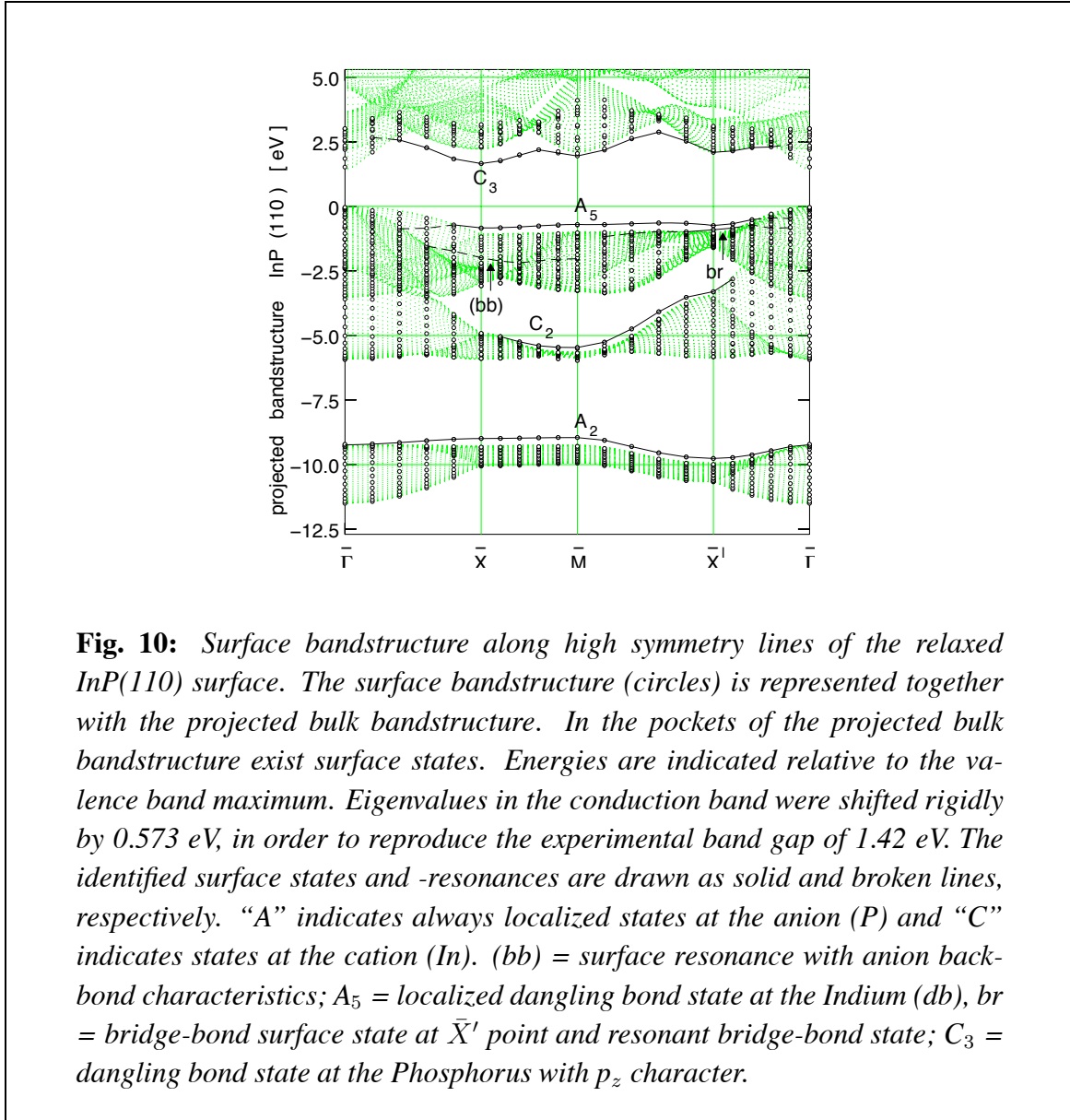
Fig. 9: Structure model for the surface relaxation of the (110) oriented surface of III-V compound semiconductors. On the lower surface the unreconstructed surface is shown. Cations are represented as white, anions as black balls.

model, the so-called *bond rotation model*. It concerns the relaxation of surface atoms in the (1×1) unit cell which is represented in Fig. 9. The surface anion (e.g. P or As) relaxes out of the surface into a distorted tetrahedral, sp^3 -hybridized environment. The surface cation relaxes towards the bulk into an approximately planar sp^2 -hybridized environment.

In Fig. 10 the surface band structure of InP(110) is shown as a typical representative of the III-V semiconductors. The underlying PBS results from bulk calculations. Overlaid are calculations of a thick finite InP(110) slab (black circles). The surface states can be identified existing in the pockets of the projected bulk bandstructure (see also Fig. 4). The surface states, which would lie in the unrelaxed case in the fundamental gap, were pushed by the relaxation to the valence- and conduction-band edge. Because of the directed bonds of the sp^3 hybrids, which determine the electronic properties of semiconductor surfaces of elemental semiconductors and III-V compound semiconductors, surface states have special names, which are related with their directionality.

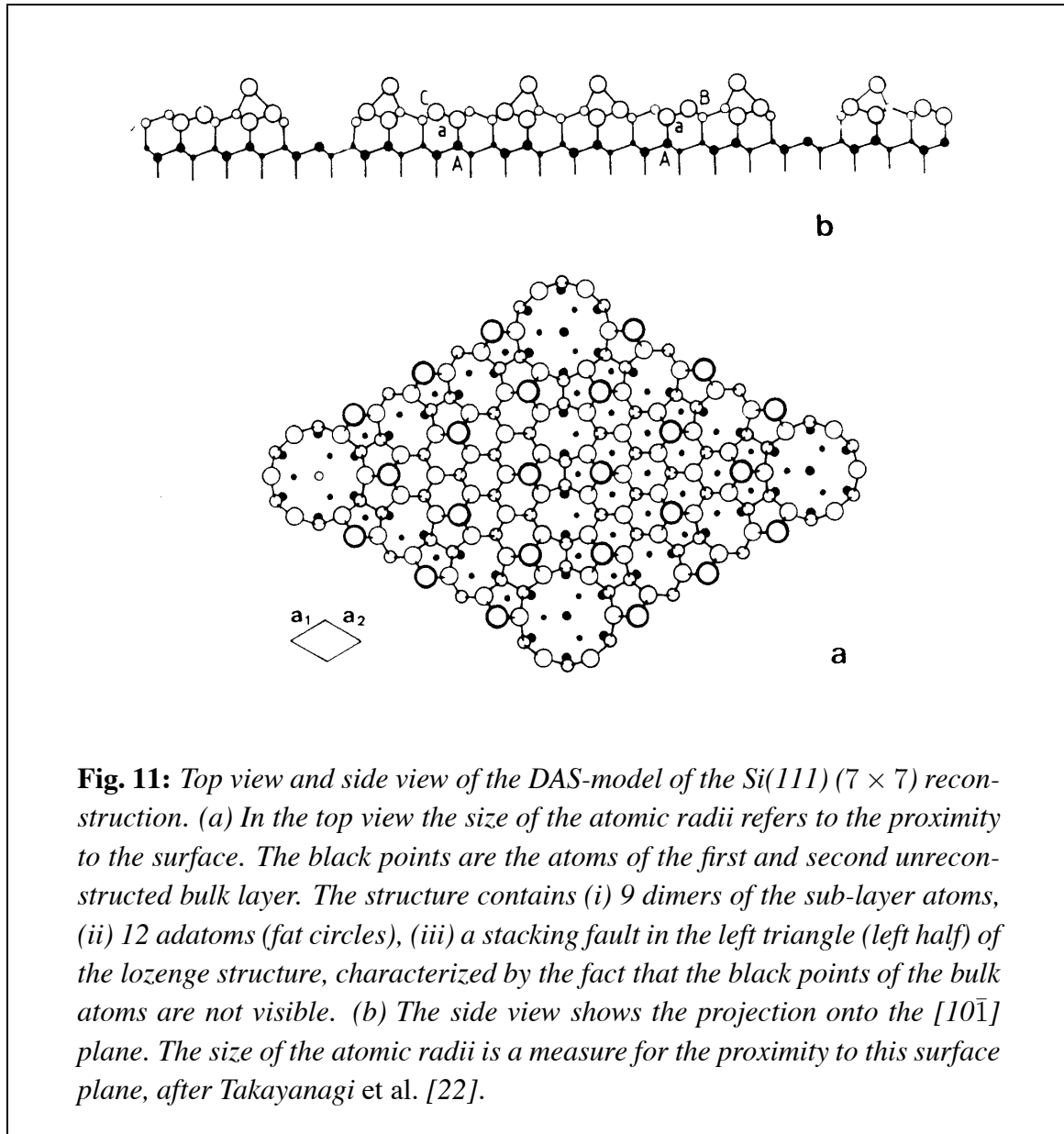
The Si(7×7) Surface

Semiconductor surfaces reconstruct nearly without exception with partially fantastic reconstructions as for example the Si(111) (7×7) reconstruction, whose structure represented a puzzle over decades and which reached a final convergence in the structure model by K. Takayanagi [22]. The suggested Dimer-Adatom-Stacking fault model (DAS-model) is shown in Fig. 11. Driving force for this reconstruction are the surface states, which are located in case of the ideal unreconstructed surface in the middle of the Si gap. The gap states are localized $3p$ dangling bond states. This is energetically an extremely unfavorable situation. By the reconstruction the new bonds are formed and the bonding changes in such a manner that the surface are shifted by hybridizing toward the band edges.



4 Transition Metals in Reduced Dimensions: Magnetism

Sofar we investigated the consequences of the reduced dimension to the electronic structure of single states, particularly around the Fermi energy. A reduction of the dimensions effects also the electronic structure as a whole. For example a reduction of the coordination number means also that the electrons have less opportunity to hop from site to site and the kinetic energy of the electron or the band width W , respectively, is reduced. Thus, the ratio of the Coulomb interaction U between the electrons on a given site and the band width, U/W , moves toward higher Coulomb interactions, and electron correlation becomes more important and the tendencies towards the appearance of magnetism or a Mott-transition is enhanced. An understanding of these phenomena requires a proper treatment of the electron-electron interaction as for example included in the various approximation of the density functional theory (DFT) or many-body



approaches of strongly correlated electrons.

As an example we explore this phenomenon here for the magnetism in transition-metals in reduced dimensions and start with observation that nearly all 30 isolated transition-metal atoms have local magnetic spin moments. The largest possible d moments occur at the center of each series, i.e. $5 \mu_B$ for Cr and Mn in the $3d$ series and the physics is well described by Hund's first rule: the spins of all d electrons are aligned in parallel up to a maximum value of $S_z = 5/2$. On the other hand, it is well-known that only 5 of 30 transition metals remain magnetic in their bulk crystalline phase: Co and Ni are ferromagnetic, Cr is antiferromagnetic, and Mn and Fe are ferromagnetic or antiferromagnetic depending on their crystal structure (cf. Fig. 12).

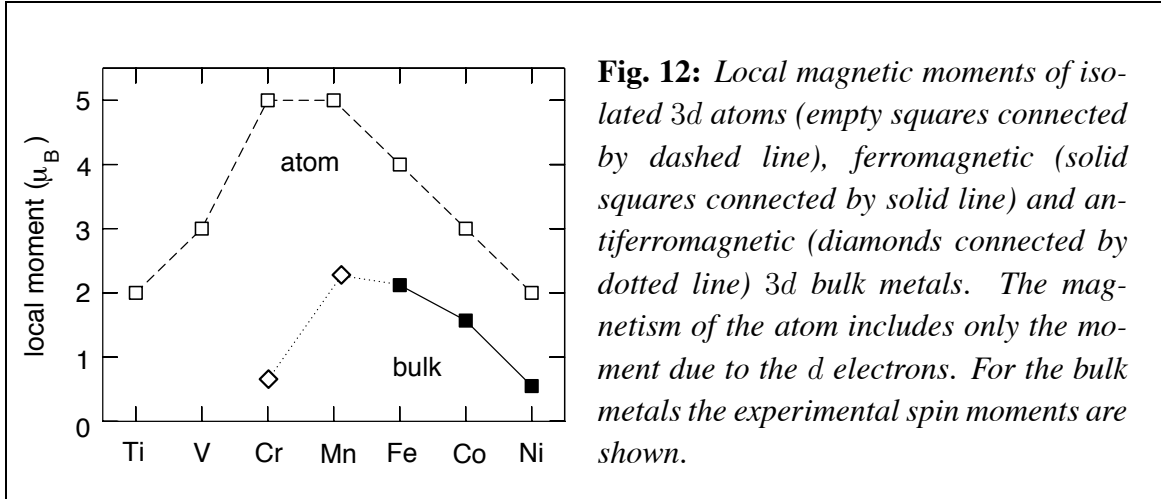


Fig. 12: Local magnetic moments of isolated 3d atoms (empty squares connected by dashed line), ferromagnetic (solid squares connected by solid line) and antiferromagnetic (diamonds connected by dotted line) 3d bulk metals. The magnetism of the atom includes only the moment due to the d electrons. For the bulk metals the experimental spin moments are shown.

Low-dimensional transition-metals should fall in between these two extremes. Magnetic material may be envisaged, which is nonmagnetic as bulk metal but magnetic as nanostructure. Although these arguments do apply, charge transfer, lift of degeneracies, structural, morphological or thermodynamical changes mire the interpolation. We focus here on the role of the band narrowing of transition-metal d bands due to the reduction of the dimensionality and its consequences for the magnetism.

4.1 Role of Coordination Number

The occurrence of ferromagnetism can be studied on the basis of the Stoner criterion:

$$I n(\varepsilon_F) > 1. \quad (26)$$

The Stoner criterion is an instability condition which expresses the competition between the exchange interaction in terms of the exchange integral I which drives the system into ferromagnetism for large I and the kinetic energy in terms of the nonmagnetic density of states (DOS) $n(\varepsilon_F)$ at the Fermi energy ε_F . The kinetic energy rises if the system becomes magnetic, the more the wider the band width or the lower the density of states, respectively. A big exchange integral and a large nonmagnetic DOS at the Fermi energy favors ferromagnetism. As explained in more detail in the lecture of G. Bihlmayer, When ferromagnetism occurs, the double degeneracy of the energy bands $\varepsilon_{\mathbf{k}}$ is lifted, majority states $\varepsilon_{\mathbf{k}\uparrow}$ and minority states $\varepsilon_{\mathbf{k}\downarrow}$ are rigidly shifted in energy by the exchange splitting IM , where M is the value of the local magnetic moment,

$$\varepsilon_{\mathbf{k}\uparrow} = \varepsilon_{\mathbf{k}} - \frac{1}{2}IM \quad \text{and} \quad \varepsilon_{\mathbf{k}\downarrow} = \varepsilon_{\mathbf{k}} + \frac{1}{2}IM. \quad (27)$$

The rigid band shift is a good model if the shift is small as in case of bulk ferromagnets. Deviations can be found for thin films or wires, as the magnetic moments and thus the exchange splitting is large.

The exchange integral I is an intra-atomic, element specific quantity, and in simplest approximation independent of the local environment, the structure and the site of a given atom, e.g.

surface atom or bulk atom. According to Gunnarsson [24] and Janak [25] a global trend

$$I_{3d} > I_{4d} > I_{5d} \quad (28)$$

was found for the exchange integrals of the $3d$, $4d$, and $5d$ transition-metal series.

Focusing on the d electrons as relevant electrons for itinerant magnetism, the DOS depends on both the coordination number N_{nn} and the hopping matrix elements h_d between the d electrons. This can be understood as follows: The energy integral $\int_W n_\ell(\varepsilon) d\varepsilon = 2\ell + 1$ over the band width, W , of the local DOS of angular momentum quantum number $\ell (= 2)$ is normalized to $2\ell + 1$ states. Thus, in simplest approximation possible (e.g. rectangular shaped DOS), one can assume that the local DOS scales inversely proportional to the band width, W ,

$$n(E_F) \sim \frac{1}{W}. \quad (29)$$

At the atomic limit the band width converges to zero, the Stoner criterion is always fulfilled and moments in accordance with Hund's first rule will be found. In general the DOS consists of contributions from electrons in s , p , d , and f states. For transition metals by far the largest contribution comes from the d electrons, and the d - d hybridization determines the shape of the density of states. Therefore, in the following discussion we restrict ourselves to d electrons and write

$$n(E_F) \approx n_d(E_F) \sim \frac{1}{W_d}. \quad (30)$$

The average local band width $\overline{W}_d(\mathbf{R}_i)$ for an atom i at position \mathbf{R}_i can be estimated in a nearest neighbor tight-binding model, applicable for the itinerant but tightly bound d electrons of transition-metal atoms, to be

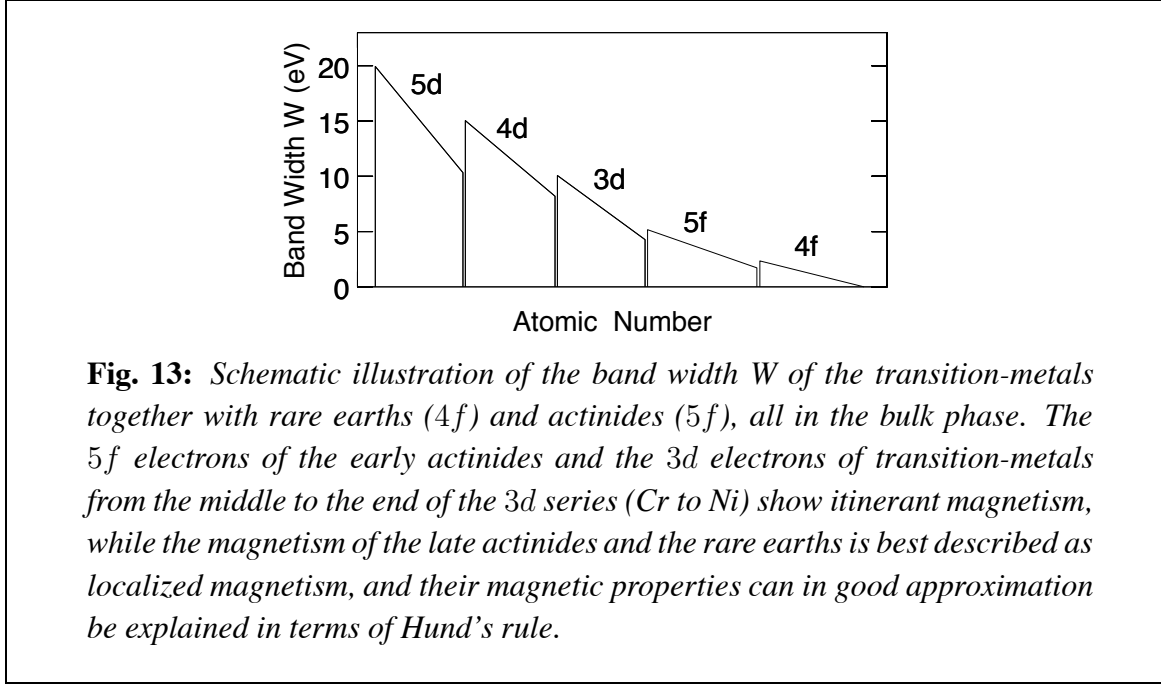
$$W_d \approx \overline{W}_d(\mathbf{R}_i) = 2 \sqrt{N_{nn}(\mathbf{R}_i)} h_d(R_{nn}). \quad (31)$$

According to equation (31) the band width depends on two quantities: (a) the hopping matrix element h_d of the d electrons and (b) the number of nearest neighbor atoms or coordination number N_{nn} .

(a) The hopping matrix element depends on the overlap of the d wavefunctions. It decreases with increasing lattice constant or distance R_{nn} to the nearest neighbor atom and for a given lattice constant it increases with the extension of the wavefunction or, equivalently, the number of nodes. In Fig. 13 the band widths of $3d$, $4d$, and $5d$ bulk transition-metals are schematically shown, together with the band widths of rare earths and actinides. In line with the arguments of increasing number of nodes from $3d$ to $5d$ wavefunctions a clear "macro trend" between the transition-metal series is visible summarized as follows:

$$h_{3d} < h_{4d} < h_{5d} \implies W_{3d} < W_{4d} < W_{5d} \implies n_{3d} > n_{4d} > n_{5d} \quad (32)$$

Within each transition-metal series there exists in addition a "micro trend": due to the incomplete screening of the Coulomb potential of the nucleus by the d electrons, the d wavefunctions at the beginning of the transition-metal series are more extended than at the end of the series, thus the hopping matrix element at the beginning of the series is larger than at the end, with the well-known consequences for the band width W and the DOS $n(E_F)$.



(b) The smaller the coordination number N_{nn} the smaller the d - d hybridization and the smaller is the band width. Let's consider for example the coordination number of an atom in the environment of a fcc crystal ($N_{fcc} = 12$), of an atom in the (001)-surface of the fcc crystal ($N_{(001)} = 8$), located in a two-dimensional (001) monolayer film ($N_{ML} = 4$) and of an atom in a monoatomic chain ($N_{chain} = 2$), keeping the nearest neighbor distance fixed ($R_{nn} = \text{constant}$) and keeping the bonding strength fixed ($h_d = \text{constant}$). Under these circumstances, one obtains for the ratio of the band widths

$$W_d^{chain} : W_d^{ML} : W_d^{(001)} : W_d^{fcc} = 0.41 : 0.58 : 0.82 : 1 ,$$

or the local DOS

$$n_d^{chain} : n_d^{ML} : n_d^{(001)} : n_d^{fcc} = 2.45 : 1.73 : 1.22 : 1 . \quad (33)$$

Thus, the reduction of the coordination number leads to less d - d hybridization, consequently to band narrowing, and in low-dimensional structures the tendency towards magnetism is considerably boosted. A nice manifestation of these arguments is reported for the size and shape dependence of the local

The reduction of the coordination number is hence responsible for the fact that the magnetism is enhanced at surfaces as compared to bulk, and the magnetism of ultrathin films should be larger than at surfaces. Accordingly, one can expect, that transition-metals, which are nonmagnetic as bulk metals, may become magnetic at surfaces or as ultra-thin films. The arguments put forward here for the increased ferromagnetism in reduced dimensions can be carried over directly to the increased antiferromagnetic susceptibility. The magnetic properties are expected to depend also on the surface or film orientation, because along with a change of the surface orientation goes a

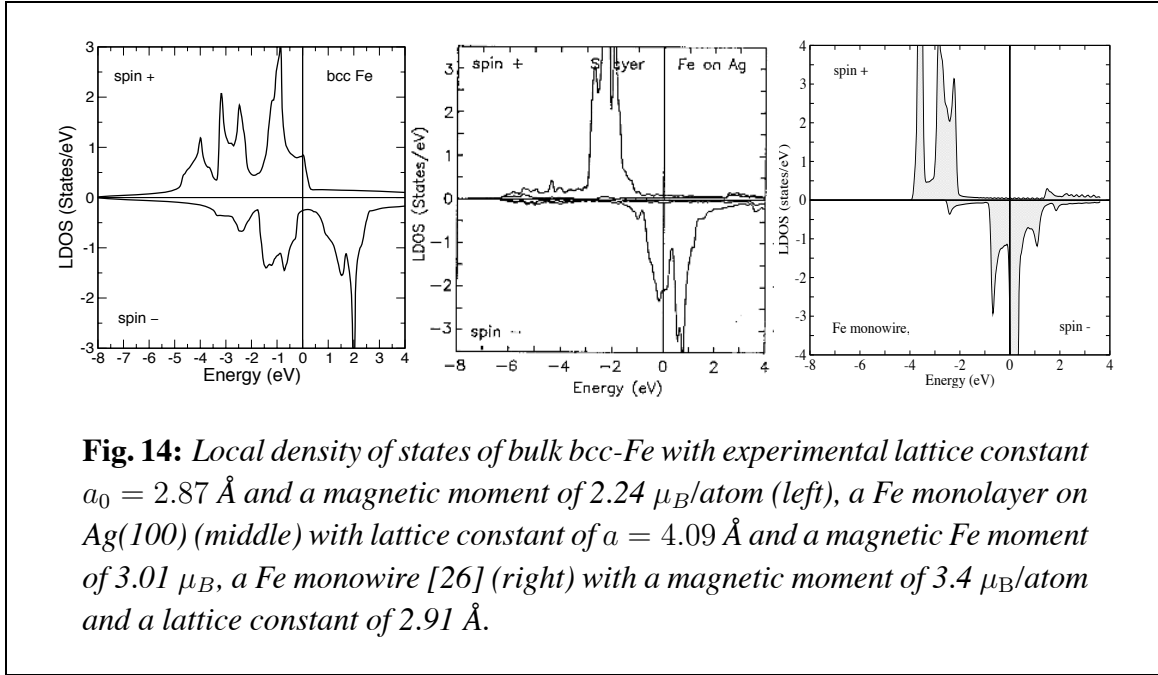


Fig. 14: Local density of states of bulk bcc-Fe with experimental lattice constant $a_0 = 2.87 \text{ \AA}$ and a magnetic moment of $2.24 \mu_B/\text{atom}$ (left), a Fe monolayer on Ag(100) (middle) with lattice constant of $a = 4.09 \text{ \AA}$ and a magnetic Fe moment of $3.01 \mu_B$, a Fe monowire [26] (right) with a magnetic moment of $3.4 \mu_B/\text{atom}$ and a lattice constant of 2.91 \AA .

Table 4: Coordination number N_{nn} , interlayer distance d , point symmetry S , and packing density ρ (fraction of the area of the surface unit cell, covered by atoms with an atom radius of touching bulk atoms) for a fcc lattice. Only the 3 low-index surfaces, (001), (011), and (111), are considered. a is the lattice parameter of the simple cubic unit cell.

	N_{nn}	S	d/a	ρ
(111)	9	C_{3v}	0.5774	0.9068
(001)	8	C_{4v}	0.5000	0.7854
(011)	7	C_{2v}	0.3536	0.5554

change of the coordination number N_{nn} (cf. Table 4) as well as a change of the nearest neighbor distance R_{\parallel} between the surface atoms and R_{\perp} between the surface atoms and the atoms in the next layer. For a fcc lattice, the (111) surface is the most densely packed one, and we expect for it the smallest enhancement of the magnetic moments. Among the three low-index surfaces, with the orientation (001), (011), and (111), the (011) surface leads to the most open surface. For the latter we expect the largest magnetic moments. At surfaces or ultrathin films of bcc lattice type the trend should be exactly the opposite. The most densely packed surface is the (011) surface for which we expected the smallest enhancements of the magnetic moments. The (111) surface is the most open one. This surface is already close to a stepped one.

The implication of the coordination number, discussed so far is the most important aspect in the magnetism of low dimensional systems.

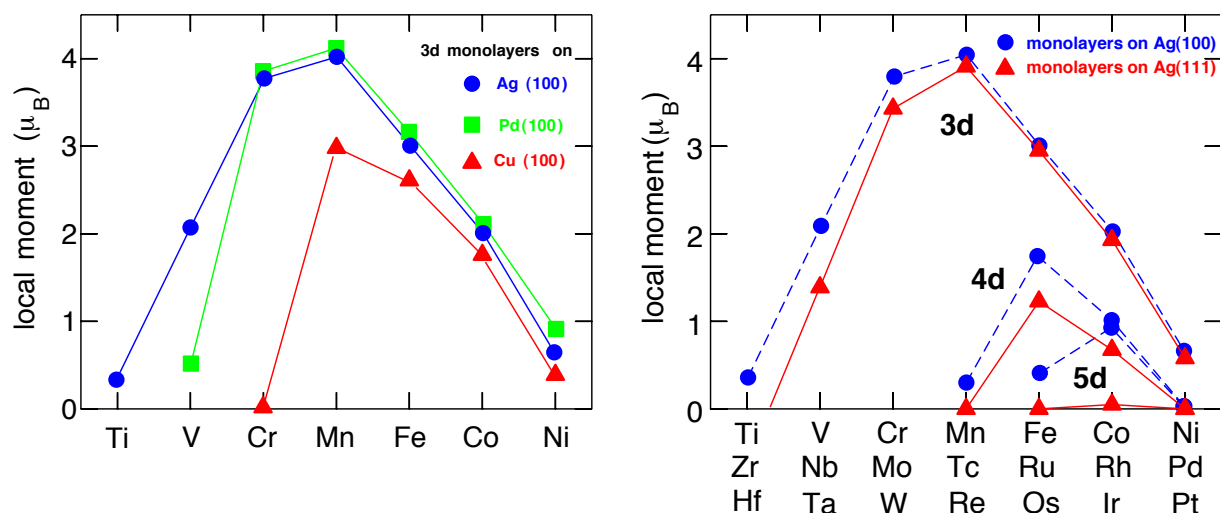


Fig. 15: Local magnetic moments as calculated for ferromagnetic (left figure) 3d-metal monolayers on Ag(100) [27] (dots), Pd(100) [28] (squares), and Cu(001) [29] (triangles), and (right figure) 3d, 4d [30], and 5d [31] monolayers on Ag(001) (dots) and Ag(111) [32] (triangles).

4.2 Low-Dimensional Magnets

The transition-metal monolayers on noble-metal substrates are the classical systems exhibiting two-dimensional (2D) magnetism. Because of the reduced coordination number of nearest neighbor transition-metal atoms in a monolayer film, the d -band width in two-dimensions is considerably smaller and correspondingly the local density of states (LDOS) at the Fermi energy E_F is considerably larger than in the bulk situation. Thus, magnetism should occur for a much wider variety of transition-metal elements. Following this line of argument it is clear that the strength of the d - d hybridization between monolayer and substrate is an additional parameter which controls the d -band width of the monolayer. For instance, large band-gap material, e.g. MgO(100), as substrate allows the formation of two-dimensional monolayer bands within the band gap of the substrate material. In this case the impact on the magnetization of the monolayer due to the substrate is expected to be small. The same is true for noble-metal substrates, which have d bands well below the Fermi energy. The width of the monolayer d band is not significantly broadened by the monolayer-substrate d - d interaction, and magnetism is restricted to the monolayer. Increasing the d - d hybridization by choosing appropriate nonmagnetic transition-metal substrates, e.g. Pd(100) or W(110), will lead to a considerable broadening of the monolayer bands and introduce a significant spin-polarization of the substrate until we have changed from the two-dimensional limit to the semi-infinite regime. Choosing a magnetic substrate an additional complexity arises due to the competition of the magnetic coupling in the monolayer and between monolayer and substrate.

A systematic investigation of the magnetism of all possible 3d, 4d, and 5d transition-metals monolayers on Ag(001) are collected in Figure 15. One finds that all 3d-metal monolayers (Ti, V, Cr, Mn, Fe, Co, Ni) on Ag(001) substrate show ferromagnetic solutions. Tc, Ru, and Rh are ferromagnetic among the 4d-metals, and Os and Ir are ferromagnetic among the 5d-metals on Ag(001). The local magnetic moments are partly very large, not only for the 3d

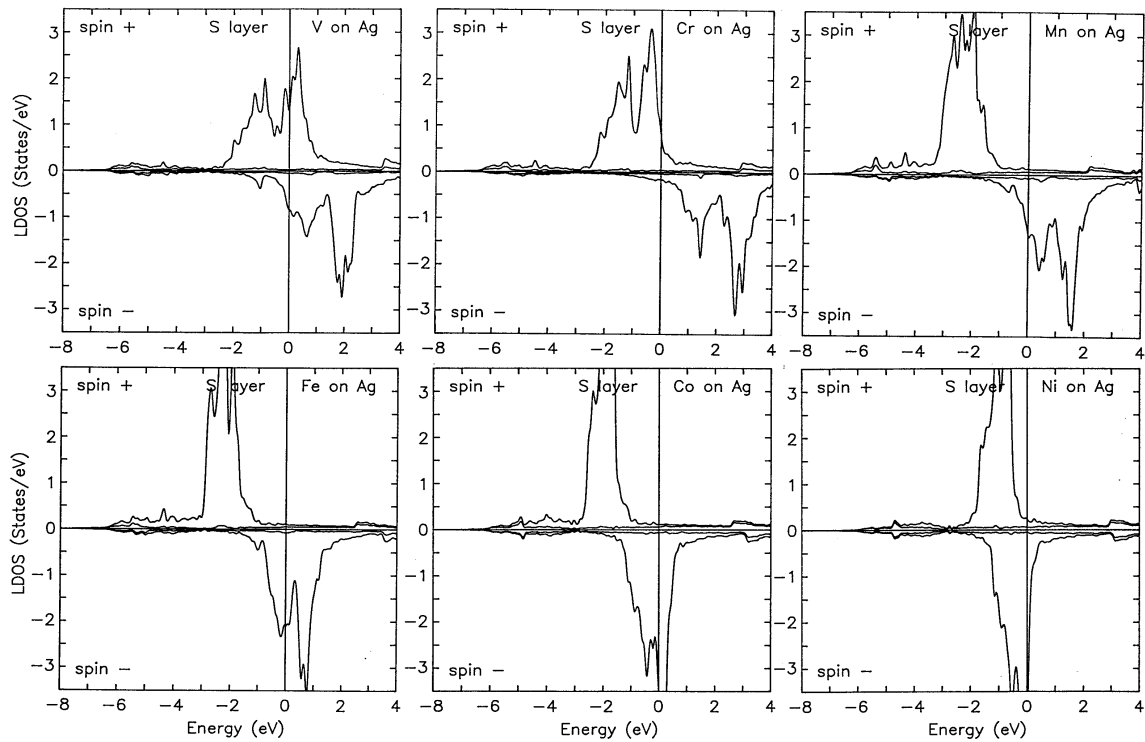


Fig. 16: Local density of states (LDOS) of ferromagnetic 3d-metal monolayers on Ag(100). The Fermi energy defines the origin of the energy scale, separating occupied (at negative energies) from unoccupied states (at positive energies). Majority (minority) states are indicated by positive (negative) values of LDOS.

monolayers, but surprisingly also for the 4d and 5d ones. In the 3d series the overall trend of the local moments follows Hund's first rule. The largest local moment of about $4 \mu_B$ was found for Mn and from Mn to Ni the magnetic moment decreases in steps of $1 \mu_B$. The latter is a consequence of the strong ferromagnetism in these monolayers. The magnetic moments of Ti, V, and Cr monolayers show a pronounced dependence on the substrate: Ti is magnetic on Ag, but nonmagnetic on Pd; the magnetic moment of V is reduced by more than $1.5 \mu_B$ when changing the substrate from Ag to Pd; and for Cr the magnetic moment changes from $3.8 \mu_B$ as an adlayer on Ag or Pd to zero as an adlayer on Cu. Although not as dramatic, the reduction is also visible for Mn. We attribute the drastic reductions of the monolayer moments to the reduction of the lattice constants in the sequence Ag to Pd to Cu.

When comparing the results of the local moments between 3d, 4d, and 5d monolayers on Ag(001) an interesting trend is observed: The element with the largest magnetic moment among each transition metal series is shifted from Mn to Ru (isoelectronic to Fe) and at last to Ir (isoelectronic to Co), respectively. Following these trends we do not expect ferromagnetism for any other 4d or 5d metal on noble metal (001) substrates, and indeed Mo and Re remained nonmagnetic. The overall picture of monolayers on Ag and Au is the same, but the different substrate interactions cause Tc and Os on Au to be nonmagnetic and lead to a slightly larger moment for Rh. Pd and Pt are predicted to be nonmagnetic. With the exception of Ru, for which

a rather small magnetic moment of $0.2\mu_B$ was calculated, no monolayer magnetism was found for $4d$ metals on Pd(100). Investigations [33] including the spin-orbit interaction have shown that the spin-orbit interactions reduces significantly the magnetic spin moment of the $5d$ -metal monolayers and depending on the interlayer relaxation the spin moment might be suppressed.

Conclusions

I presented a simple introduction to the field of electronic structure at reduced dimensions. Few things had been said, many topics were left out such as the Rashba physics of electrons in structure asymmetric environments, the electronic structure of fullerenes, carbon nanotubes, graphene, molecular magnets etc.

Acknowledgment

I thank Gustav Bihlmayer for many fruitful discussions and Alexander Hanuschkin for some valuable help in the preparation of the manuscript.

References

- [1] T. Miller, A. Samsavar, G.E. Franklin, and T.-C. Chiang, Phys. Rev. Lett. **61**, 1404 (1988).
- [2] C. Carbone, E. Vescovo, O. Rader, W. Gudat, W. Eberhardt, Sol. State Comm. **100**, 749 (1996).
- [3] B. Engels, Dissertation RWTH-Aachen (1996).
- [4] B. Engels, P. Richard, K. Schroeder, S. Bügel, Ph. Ebert, and K. Urban, Phys. Rev. B. **58**, 7799 (1998).
- [5] A. Euceda, D. M. Bylander und L. Kleinman, Phys. Rev. B **28**, 528 (1983).
- [6] W. Shockley, Phys. Rev. **56**, 317 (1939).
- [7] I.E. Tamm, Phys. Z. Soviet Union **1** 732 (1932).
- [8] S.D. Kevan, Phys. Rev. Lett. **50**, 526 (1983).
- [9] P. Heimann, J. Hermanson, H. Misoga und H. Neddermeyer, Phys. Rev. B **20**, 3059 (1979).
- [10] S.D. Kevan und R.H. Gaylord, Phys. Rev. B **36**, 5809 (1987).
- [11] F. Reinert, G. Nicolay, S. Schmidt, D. Ehm, and S. Hufner, Phys. Rev. B **63**, 115415 (2001).

- [12] J.A. Stroschio, D.T. Pierce, A. Davies, R.J. Celotta und M. Weinert, Phys. Rev. Lett. **75**, 2960 (1995).
- [13] A. Davis, J. A. Stroschio und R. J. Celotta, Phys. Rev. Lett. **76**, 4175 (1996).
- [14] A. Biedermann, O. Genser, W. Hebenstreit, M. Schmid, J. Redinger, R. Podloucky und P. Varga, Phys. Rev. Lett. **76**, 4179 (1996).
- [15] H. Mönig, J. Sun, Yu. M. Koroteev, G. Bihlmayer E. V. Chulkov, K. Pohl, and Ph. Hofmann, Phys. Rev. B **72**, 085410 (2005).
- [16] C. S. Søndergaard, PhD Thesis, University of Aarhus, Denmark (2001)
- [17] Yu. M. Koroteev, G. Bihlmayer, J. E. Gayone, E. V. Chulkov, S. Blügel, P. M. Echenique, and Ph. Hofmann, Phys. Rev. Lett. **93**, 046403 (2004).
- [18] G. Bihlmayer, Yu. M. Koroteev, P. M. Echenique, E. V. Chulkov, and S. Blügel, Surf. Sci. **600**, 3888, (2006).
- [19] J. I. Pascual, G. Bihlmayer, Yu. M. Koroteev, H.-P. Rust, G. Ceballos, M. Hansmann, K. Horn, E. V. Chulkov, S. Blügel, P. M. Echenique, Ph. Hofmann, Phys. Rev. Lett. **93**, 196802 (2004).
- [20] J. Sun, A. Mikkelsen, M. Fuglsang Jensen, Y. M. Koroteev, G. Bihlmayer, E. V. Chulkov, D. L. Adams, Ph. Hofmann, and K. Pohl, Phys. Rev. B **74**, 245406 (2006).
- [21] Ph. Hofmann, J. E. Gayone, G. Bihlmayer, Yu. M. Koroteev, and E. V. Chulkov, Phys. Rev. B **71**, 195413 (2005).
- [22] K. Takayanagi, Y. Tanishiro, S. Takahashi, M. Takahashi, Surf. Sci. **164**, 367 (1985).
- [23] R. H. Gaylord, K. H. Jeong und S. D. Kevan, Phys. Rev. Lett. **62**, 2036 (1989).
- [24] O. Gunnarsson, J. Phys. F: Met. Phys. **6**, 5876 (1976).
- [25] J.F. Janak, Phys. Rev. B **77**, 255 (1977).
- [26] Y. Mokrousov, G. Bihlmayer and S. Blügel, Phys. Rev. B. **72**, 045402 (2005).
- [27] S. Blügel and P. H. Dederichs, Europhys. Lett. **9**, 597 (1989).
- [28] S. Blügel, Europhys. Lett. **7**, 743 (1988).
- [29] S. Blügel, Appl. Phys. A **63**, 595 (1996).
- [30] S. Blügel, Europhys. Lett. **18**, 257 (1992).
- [31] S. Blügel, Phys. Rev. Lett. **68**, 851 (1992).
- [32] J. Redinger, R. Podloucky, S. Blügel, Phys. Rev. B **51**, 13582, (1995).
- [33] B. Újfalussy, L. Szunyogh, and P. Weinberger, Phys. Rev. B **51**, 12836 (1995).